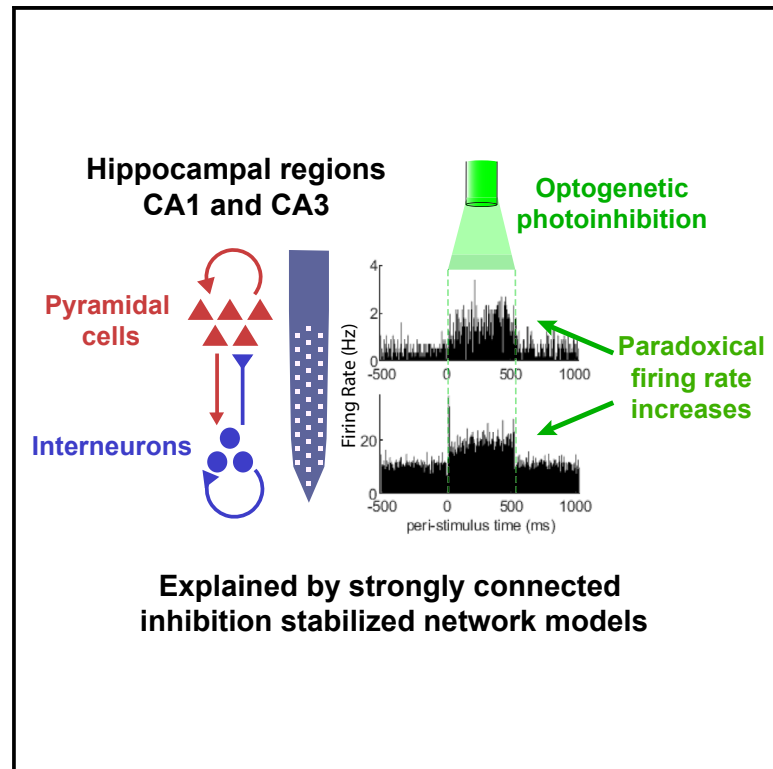


Current Biology

Optogenetics reveals paradoxical network stabilizations in hippocampal CA1 and CA3

Graphical abstract



Authors

Laurel Watkins de Jong,
 Mohammadreza Mohagheghi Nejad,
 Euisik Yoon, Sen Cheng, Kamran Diba

Correspondence

kdiba@umich.edu

In brief

Watkins de Jong et al. observed off-target and paradoxical neuronal responses to optogenetics in hippocampal CA1 and CA3, with increased firing during photoinhibition and decreased firing during photoexcitation. They show that these effects are explained by a class of network models in which strong recurrent excitation is stabilized by inhibition.

Highlights

- Optogenetics produce off-target paradoxical responses in CA1 and CA3
- Photoinhibition of CA3 produces increased firing in downstream CA1 interneurons
- Strong excitatory recurrent connectivity drives dynamics in both CA1 and CA3
- Inhibitory-stabilized network models of CA1 and CA3 can account for these effects



Article

Optogenetics reveals paradoxical network stabilizations in hippocampal CA1 and CA3

Laurel Watkins de Jong,^{1,2} Mohammadreza Mohagheghi Nejad,³ Euisik Yoon,⁴ Sen Cheng,³ and Kamran Diba^{1,2,5,6,7,*}¹Department of Anesthesiology, Michigan Medicine, 1150 W. Medical Center Dr, Ann Arbor, MI 48109, USA²Department of Psychology, University of Wisconsin—Milwaukee, 2441 E Hartford Ave, Milwaukee, WI 53211, USA³Institute for Neural Computation, Ruhr University Bochum, Universitätsstr. 150, 44801 Bochum, Germany⁴Department of Electrical Engineering and Computer Science, 1301 Beal Avenue, University of Michigan, Ann Arbor, MI 48109, USA⁵Neuroscience Graduate Program, University of Michigan, Ann Arbor, MI 48109, USA⁶Twitter: @SharpWaveRipple⁷Lead contact

*Correspondence: kdiba@umich.edu

<https://doi.org/10.1016/j.cub.2023.03.032>

SUMMARY

Recurrent connectivity between excitatory neurons and the strength of feedback from inhibitory neurons are critical determinants of the dynamics and computational properties of neuronal circuits. Toward a better understanding of these circuit properties in regions CA1 and CA3 of the hippocampus, we performed optogenetic manipulations combined with large-scale unit recordings in rats under anesthesia and in quiet waking, using photoinhibition and photoexcitation with different light-sensitive opsins. In both regions, we saw striking paradoxical responses: subsets of cells increased firing during photoinhibition, while other cells decreased firing during photoexcitation. These paradoxical responses were more prominent in CA3 than in CA1, but, notably, CA1 interneurons showed increased firing in response to photoinhibition of CA3. These observations were recapitulated in simulations where we modeled both CA1 and CA3 as inhibition-stabilized networks in which strong recurrent excitation is balanced by feedback inhibition. To directly test the inhibition-stabilized model, we performed large-scale photoinhibition directed at (GAD-Cre) inhibitory cells and found that interneurons in both regions increased firing when photoinhibited, as predicted. Our results highlight the often-paradoxical circuit dynamics that are evidenced during optogenetic manipulations and indicate that, contrary to long-standing dogma, both CA1 and CA3 hippocampal regions display strongly recurrent excitation, which is stabilized through inhibition.

INTRODUCTION

The distinct neuroarchitecture of the hippocampus inspires speculation about the computational features of its circuitry. The dominant pattern of connections within this (so-called “tri-synaptic”) circuit suggests sequential processing through the dentate gyrus (DG), cornu ammonis 3 (CA3), and cornu ammonis 1 (CA1) regions, with the latter providing the output node of the hippocampus, even though the presence of direct inputs from the entorhinal cortex and other brain regions at each of these nodes indicates a more complicated picture.^{1,2} The CA regions in particular feature a dense layer of pyramidal neurons that stretches from the hilus region of the DG out toward the subiculum. But while CA3 features extensive recurrent connections between its pyramidal cells (pyr), CA1 has largely been considered to be feedforward, with few direct intralaminar connections. Furthermore, distinct subtypes of interneurons (int) connect to these pyramidal cells, as well as to each other, both within and across these subregions.³

Understanding the computational properties of these microcircuits is a challenge that has important implications for understanding how the hippocampus supports memory. The

advent of optogenetic techniques that combine photo-sensitive opsins with targeted light delivery for manipulating the activity of neurons has provided an important and powerful method for probing neuronal circuits to arrive at a better understanding of their underlying dynamics.⁴ Many studies employ these circuit manipulations in the context of behavior, to test hypotheses concerning the causal roles of specific neuronal subpopulations in mediating different behaviors. In the hippocampus, these studies infer important mnemonic roles for different hippocampal subpopulations. However, optogenetic manipulations are not typically combined with neuronal recordings or, if they are, the recordings do not often extend beyond the site of photo illumination. Nevertheless, as an increasing number of investigations combine optogenetic manipulations with recordings of neuronal activity, a rich repertoire of network dynamics has emerged, including in off-target neurons.^{5–11} As these studies have shown, the responses of targeted and off-target neurons to perturbations can provide valuable insights into the motifs operating in different circuits.

In this study, we set out to probe the dynamics of microcircuits in regions CA1 and CA3 by performing optogenetic manipulations of neurons while recording extracellular spikes



from neurons targeted with light as well as neurons distal to the light source. Rather than simple firing suppression upon optogenetic photoinhibition, or increased excitation upon optogenetic photostimulation, we found that our manipulations produced unexpected and paradoxical effects in these circuits, particularly in neurons further away from the source of light, which are rarely considered when interpreting findings from optogenetics studies. We replicated our observations with a variety of different opsins and opto-electrode interfaces, including both photoinhibition and photostimulation. To better understand our observations, we developed a spiking computational model based on inhibition-stabilized networks (ISNs), as first described by Tsodyks et al.,¹² in which inhibitory connections play a key role in balancing runaway excitation caused by strong recurrence between excitatory neurons. We found that this class of model can provide an explanation for the neuronal dynamics revealed by optogenetics, not only in hippocampal CA3, which is known to be strongly recurrent, but surprisingly also in CA1, which has been widely suggested to be feedforward. Our work therefore indicates that both CA3 and CA1 behave as inhibitory-stabilized networks, with significant implications for the class of computations performed in these regions.¹³

RESULTS

Photoinhibition in CA1 and CA3 results in paradoxical disinhibition of a subset of pyramidal cells and interneurons

To examine the response of CA1 and CA3 networks to optogenetic perturbation, we infused a photoinhibitory AAV2-CamKII α -ArchT-GFP opsin vector into the dorsal CA1 and contralateral CA3b regions of rats (Figure S1). We then examined perturbations in each region using integrated optic fiber silicon probe optrodes¹⁴ for simultaneous recordings and light delivery in rats (Figure 1A) under urethane anesthesia, which induces firing activity patterns and activity levels similar to those seen during natural waking and sleep.^{15–17} We examined activities in pyramidal cells and interneurons, putatively separated using quadratic discriminant analysis based on standard criteria involving waveshapes and inter-spike intervals (Figure S2; also see Table S1 for a summary of different sessions and experiments performed in this study). We tested each cell separately for significant firing changes during the light-on period compared with a pre-light baseline period of the same duration, excluding 20 ms centered on the light onset (binomial test). As an additional control, we compared experimental results against expected null observations derived from comparing two non-overlapping pre-light baseline periods (“baseline null,” STAR Methods; see Figures S3 and S4; Table S2). In experiments targeting CA1 ($n = 3$ rats, 6 sessions) we observed decreased firing at the site (electrode shank) of the optical fiber in pyramidal neurons (Figures 1A and 1B), as expected. Putative inhibitory interneurons also decreased firing, reflecting non-specific expression of the CamKII α promoter in hippocampal neurons.^{18,19} But inconsistent with a purely photoinhibitory role for ArchT, at silicon probe sites 600 μm away laterally from the optical light source, a proportion of both pyramidal cells and interneurons displayed significantly increased firing in response to light pulses.

Such non-local firing responses presumably arise from circuit interactions between excitatory and inhibitory neurons. Therefore, we tested whether perturbations in region CA3b ($n = 3$ rats, 6 sessions), which displays different circuit connection motifs than CA1,¹ would produce a similar effect (Figure 2). In these CA3b experiments, we also observed a net decrease in firing in response to photoinhibition; however, compared with CA1, a larger proportion of cells showed significantly increased firing during light-on periods. Not only did neurons on silicon probe shanks 600 μm away from the optical fiber (19/35 pyr, 20/63 int) increase firing significantly in response to light, but even at electrode sites near the optic fiber some neurons displayed significantly enhanced firing (6/36 pyr, 5/37 int). On a neighboring silicon probe shank just 200 μm away from the optical fiber, the typical response was strongly increased firing—particularly in pyramidal cells (19/41 pyr) but also in interneurons (7/33 int). In sum, networks in both region CA1 and CA3b displayed a paradoxical increased firing response to photoinhibition at a nearby site, though between the two regions the strength of this effect scaled differently with distance from the site of illumination.

One potential concern is that these observations may not be due to circuit effects but rather disrupted biophysics resulting from optogenetic vectors. In particular, it has been reported that optical illumination can trigger Ca²⁺ influx in axonal tissue expressing the ArchT opsin, potentially resulting in vesicular release²⁰ that is depolarizing rather than suppressive (but see also El-Gaby et al.²¹). However, this was unlikely to be a confound in our experiments because our illumination periods were brief compared with the minutes-long, light-on periods that evoked Ca²⁺ influx in that study.²⁰ Furthermore, the neuronal responses we observed were temporally locked to the onsets and offsets of illumination. In contrast, the axonal Ca²⁺ influxes associated with ArchT take minutes to rise and last for minutes beyond the illumination offset.²⁰ Nevertheless, to ensure the robustness of our observations, we repeated experiments in CA3b using an alternative photoinhibitory opsin, the soma-targeted anion-conducting channelrhodopsin (stGtACR2) vector, alongside a blue light source for an 8-shank optoelectrode (STAR Methods). These experiments produced very similar results (Figure S5), with disinhibition particularly on electrodes away from the optical fiber, which appears inconsistent with a purely neuro-suppressive role for photoinhibitory opsins.

To further test whether these unexpected responses require strong light stimulation that might disperse throughout neuronal tissue, in another set of experiments using AAV1-CamKII α -stGtACR2-fusionRed, we examined network responses to optogenetic manipulation that was restricted to very small subsets of neurons using monolithically integrated- μLED silicon probes, allowing for low-power focal optical illumination combined with simultaneous extracellular recordings²² (Figure 3). In these experiments, we illuminated only a single μLED at a time, setting it to the lowest power setting that still elicited a visible neuronal response (typically 50–80 μA) on unit spikes from nearby recording electrodes. Despite the restricted optical illumination and the use of a soma-targeting opsin in these experiments, a subset of neurons on silicon probe shanks away from the illumination site showed significantly increased activity during photoinhibition. In both CA1 and CA3b, both pyramidal cells (CA1: $p = 0.0249$

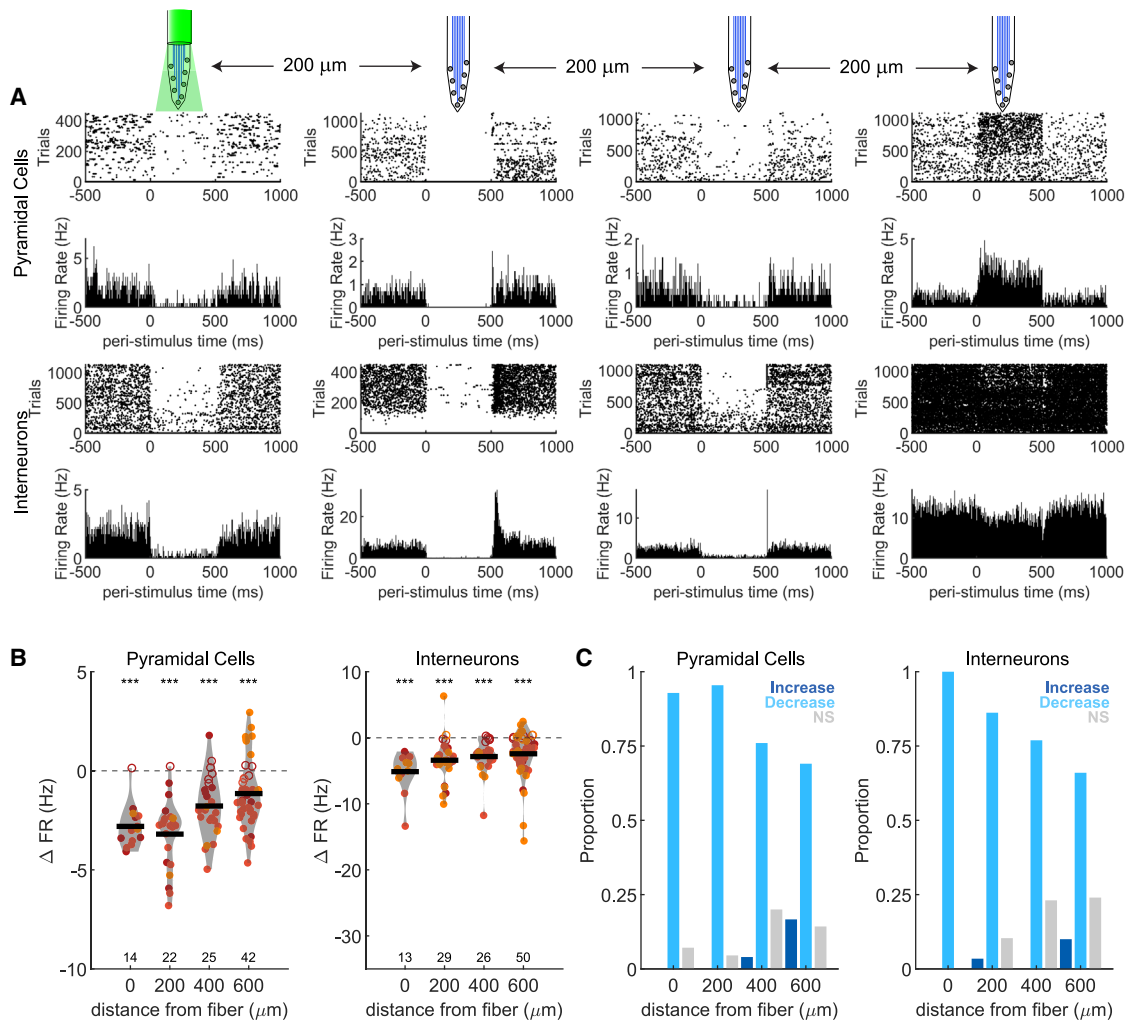


Figure 1. Local and off-target effects of photoinhibition in CA1

Optrode responses recorded in neurons of animals infused with CamKII α -ArchT in CA1.

(A) Example responses of pyramidal cells and interneurons at the location of the fiber and at increasing distances from the site of a 500-ms illumination. The top panels show spike rasters for multiple trials centered on the illumination period, while the bottom panels show peri-event histograms across these trials. Note example of a pyramidal cell recorded 600 μm away from the illumination fiber that shows increased firing.

(B and C) (B) Population firing rate changes and (C) proportion plots for pyramidal cells (left) and interneurons (right) as a function of distance from the optic fiber. Individual cells overlaid on the population violin plots are colored according to animal, with the black horizontal line providing the group mean. Filled circles identify significantly modulated cells (binomial test, $\alpha = 0.01$). Numbers at the bottom of each panel provide the number of cells in each condition. A large proportion of pyramidal cells showed decreased firing at the site of illumination as well as at more distal sites. Similarly, a large proportion of interneurons showed decreased firing at the site of illumination and further away from the fiber. However, a small proportion of both pyramidal cells and interneurons showed significantly increased firing rates, particularly at sites most distal from the optical fiber. *** $p < 0.0001$, paired t test. See [Figure S3](#) and [Tables S2](#) and [S3](#) for comparisons with null baselines.

at 400 μm ; CA3: $p < 0.05$ at all sites, Fisher's exact tests compared with baseline null, see [Table S2](#)) and interneurons (CA1: $p < 0.05$ at 200 and 400 μm ; CA3: $p < 0.05$ at 0, 200, and 400 μm ; Fisher's exact tests compared with baseline null) showed a disinhibitory response. This disinhibitory response was generally stronger in CA3b ($p = 2.20\text{e-}16$ for pyr and $p = 5.92\text{e-}4$ for int; Fisher's exact tests of the proportion of increased firing cells pooled across distances, compared between CA3 and CA1) and for CA3 was present in both pyramidal cells and interneurons ($p = 4.31\text{e-}12$ for pyr and $p = 8.81\text{e-}6$ for int, Fisher's exact test for at 0 μm

site compared with baseline null) even within the same electrode shank as the illuminating μLED .

Photostimulation in CA1 and CA3 produces paradoxical suppression of firing in a subset of pyramidal cells and interneurons

Our experiments thus far tested the effects of *photoinhibition*. We then asked whether *photostimulation* using an excitatory opsin would generate complementary paradoxical responses. We infused AAV5-hSyn-oChIEF-tdTomato, a photoexcitatory channelrhodopsin with modified kinetics, into dorsal CA1 and

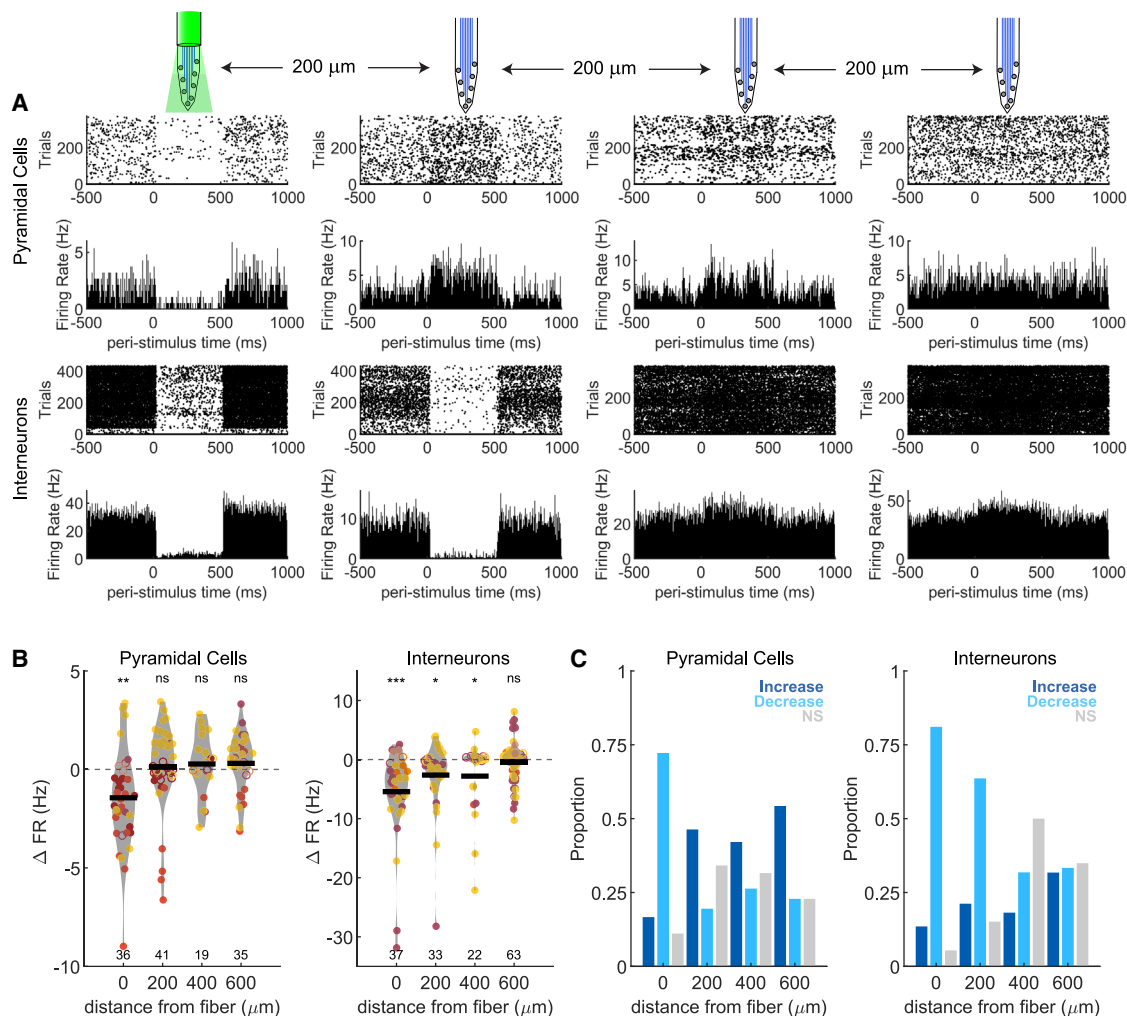


Figure 2. Local and off-target effects of photoinhibition in CA3

Optrode responses recorded in neurons of animals infused with CamKII α -ArchT in CA3.

(A) Example responses of pyramidal cells (top) and interneurons (bottom) at the location of the fiber and at increasing distances from the site of illumination. The top panels show spike rasters for multiple trials centered on the illumination period, while the bottom panels show peri-event histograms across these trials. Note multiple examples of cells recorded away from fiber that show increased firing in response to the illumination.

(B and C) (B) Population firing rate changes and (C) proportion plots for pyramidal cells (left) and interneurons (right) as a function of distance from the optic fiber. Individual cells overlaid on the population violin plots are colored according to animal, with the black horizontal line providing the group mean. Filled circles identify significantly modulated cells (binomial test, $\alpha = 0.01$). Numbers at the bottom of each panel provide the number of cells in each condition. A large proportion of cells showed a significant change in spiking activity during photo illumination, with some decreasing firing but many others instead increasing (see Figure S5 for similar results with the CamKII α -stGTACR2 opsin). * $p < 0.01$, ** $p < 0.001$, *** $p < 0.0001$, paired t test. See Figure S3 and Tables S2 and S3 for comparisons with null baselines.

contralateral CA3b²³ and again performed recordings and stimulation using the μ LED probes ($n = 4$ rats, 9 sessions). In these experiments (Figure 4), we expected an increased firing response to photostimulation, and indeed, near the stimulation response, we observed higher firing in both pyramidal cells and interneurons during μ LED illumination. However, notably consistent with the complex responses in the photoinhibition experiments, a subset of cells in both CA1 and CA3b showed a firing decrease during photostimulation. Although the proportion of cells that showed decreased firing was higher away from the μ LED site, particularly in CA3b (e.g., note the large proportions of pyr with decreased firing at 400 and 600 μm in

Figure 4E; $p = 0.0485$ and $p = 0.0408$, respectively, Fisher's exact test compared with baseline null; see also similar results obtained from the model in a subsequent section), even on the same recording electrode shank as the stimulating μ LED, we observed significantly decreased firing in a subset of pyramidal cells and interneurons, though the total number were too few to reach significance ($p = 0.11$ for pyr and $p = 0.10$ for int, Fisher's exact tests compared with baseline null). This observation indicates that circuit responses that are incompatible with a unidirectional effect of optogenetics occur under both photostimulation and photoinhibition, including when very small numbers of neurons are perturbed.

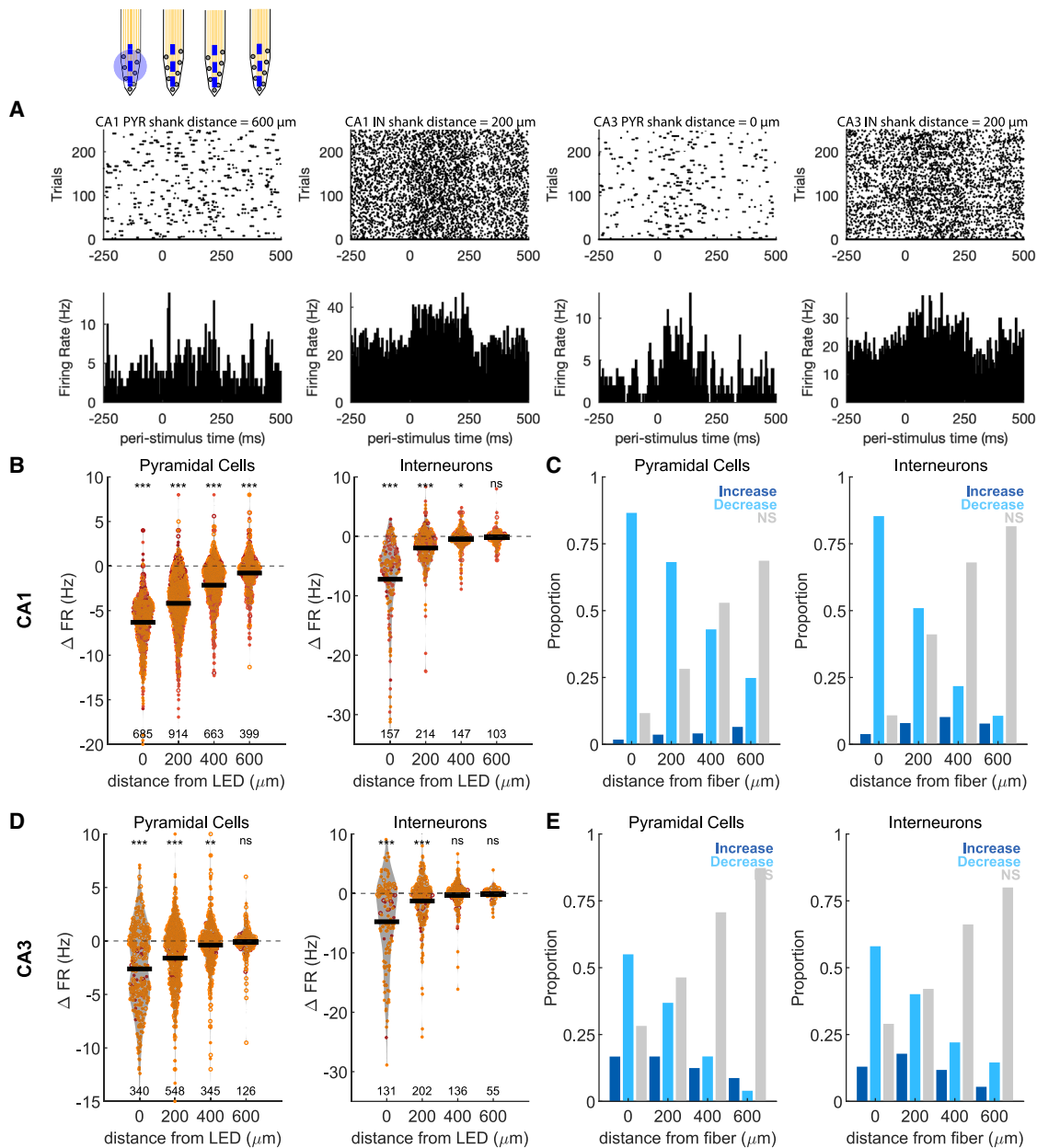


Figure 3. Response profile of focal μLED photoinhibition in CA1 and CA3

Focal photoinhibition with μLED optoelectrodes in animals expressing CamKII α -stGtACR2 in CA1 and CA3.

(A) Example rasters (top) and peri-stimulus histograms (bottom) obtained from units on electrode shanks at varying distances from the light source μLED . From left to right, the panels show spike times surrounding multiple trials of a 250-ms μLED illumination period for a pyramidal cell and an interneuron in CA1, and a pyramidal cell and an interneuron in CA3. The distances of the unit shank from the μLED shanks are indicated above each raster.

(B and C) (B) Population firing rate changes and (C) proportion plots for CA1 pyramidal cells (left) and interneurons (right) as a function of distance from the μLED shank generally showed significant decreases in firing rate at all sites in response to low-level focal illumination. Individual cells overlaid on the population violin plots are colored according to animal, with the black horizontal line providing the group mean. Filled circles identify significantly modulated cells (binomial test, $\alpha = 0.01$). Numbers at the bottom of each panel provide the number of cells in each condition. Consistent with the fibered optrode experiments using ArchT, a small subset of cells showed increased firing at sites away from the μLED .

(D and E) (D) Population firing rate changes and (E) proportion plots for CA3 pyramidal cells (left) and interneurons (right) as a function of distance from the μLED shank mostly showed decreased firing. The proportion of pyramidal cells and interneurons with increased firing in response to the photo illumination was prominent, including even on the same electrode shank as the illuminated μLED (see Figure S5 for results with the fiber-coupled optrode). * $p < 0.01$, ** $p < 0.001$, *** $p < 0.0001$, paired t test.

See Figure S3 and Tables S2 and S3 for comparisons with null baselines.

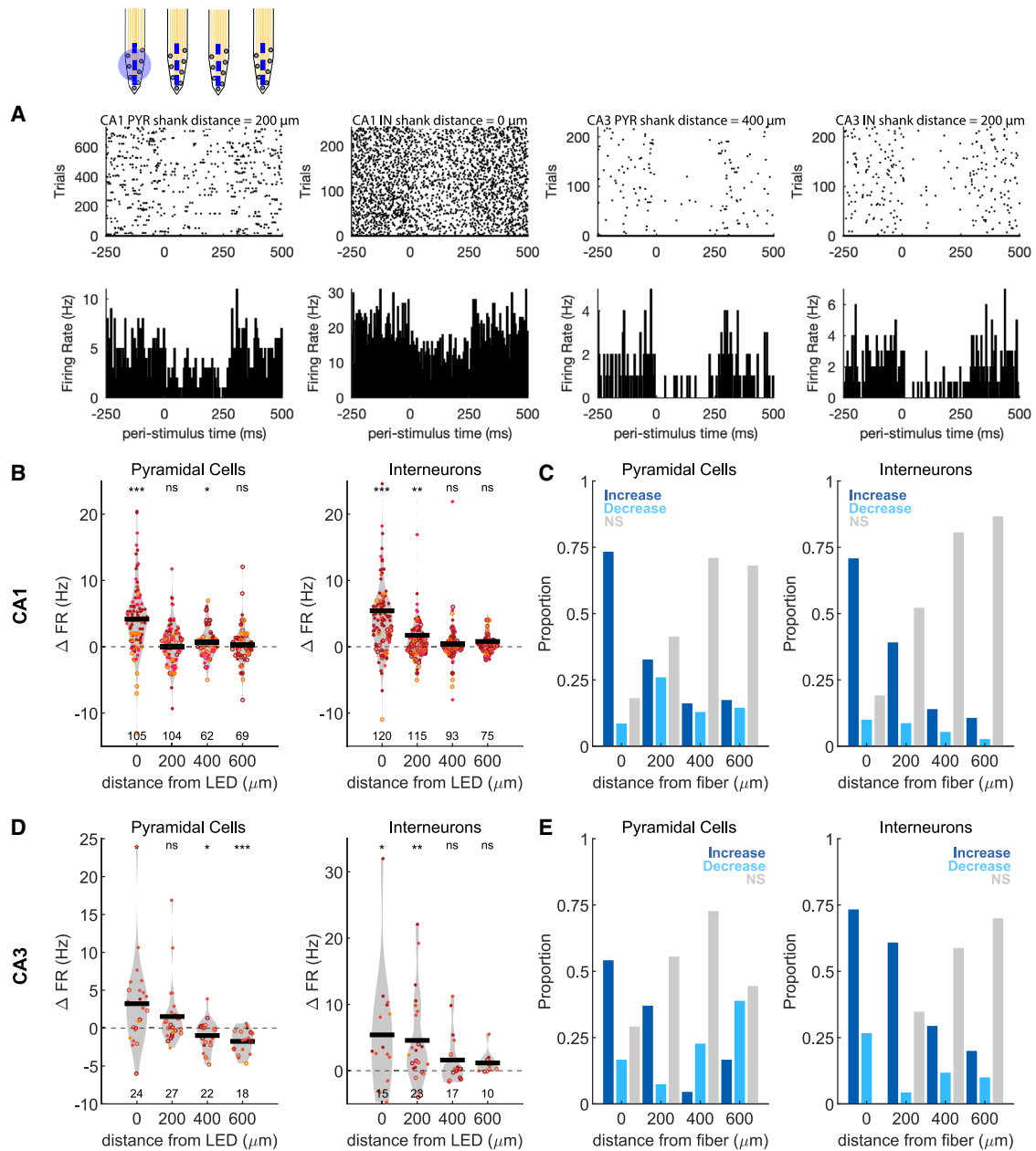


Figure 4. Response profile of focal μLED photostimulation in CA1 and CA3

Focal photostimulation with μLED optoelectrodes in animals expressing hSyn-oCHIEF in CA1 and CA3 neurons.

(A) Example rasters (top) and peri-stimulus histograms (bottom) obtained from units on electrode shanks at varying distances from the light source μLED . From left to right, the panels show spike times surrounding multiple trials of a 250-ms μLED illumination period for a pyramidal cell and an interneuron in CA1, and a pyramidal cell and an interneuron in CA3. The distances of the unit shank from the μLED shanks are indicated above each raster.

(B and C) (B) Population firing rate changes and (C) proportion plots for CA1 pyramidal cells (left) and interneurons (right) as a function of distance from the μLED shank generally showed significant firing increases in response to low-level focal stimulation. Individual cells overlaid on the population violin plots are colored according to animal, with the black horizontal line providing the group mean. Filled circles identify significantly modulated cells (binomial test, $\alpha = 0.01$). Numbers at the bottom of each panel provide the number of cells in each condition. Although most cells increased firing, as expected, a small subset of cells at different distances away from the μLED also showed decreased firing in response to the photostimulation as seen in the example panels.

(D and E) (D) Population firing rate changes and (E) proportion plots for CA3 pyramidal cells (left) and interneurons (right) as a function of distance from the μLED shank showed similar responses. * $p < 0.01$, ** $p < 0.001$, *** $p < 0.0001$, paired t test.

See Figure S3 and Tables S2 and S3 for comparisons with null baselines.

In summary, in both photoinhibition and photostimulation experiments we observed a heterogeneous response in pyramidal cells and interneurons, both distal to and near the site of illumination. Together, these data suggest that hippocampal networks in both CA1 and CA3b generate non-local responses to optogenetic illumination that are often in the opposite direction from the presumed action of the optogenetic manipulation, with disinhibition during photoinhibition and suppression during photostimulation.

CA1 and CA3b behave as inhibitory-stabilized networks

These paradoxical network responses do not readily fit expectations derived from optogenetic manipulations on single cells. However, Tsodyks et al.¹² previously described similarly paradoxical responses in strongly connected networks, where an inhibitory population must act to stabilize potential runaway activity arising from the recurrent excitatory connections, thereafter called—as previously mentioned—ISNs. Since then, inhibition stabilization has been proposed to provide a frequent motif for circuit operations throughout the neocortex,^{7,8} though there is an ongoing debate and possible exceptions.^{5,10} Although ISNs were originally proposed to account for the theta phase alignment of interneurons with pyramidal cells in hippocampal CA1, there has yet to be a direct test of inhibition stabilization in a hippocampal region. In ISNs, decreased input drive to inhibitory cells causes an increase in the excitation of the network, which then paradoxically increases the firing of the inhibitory cells. Our results thus far appear to be consistent with ISNs in both CA1 and CA3, though a potential caveat remains that interactions between different inhibitory subtypes can also produce unexpected firing patterns, even in a weakly recurrent non-ISN.^{10,24} Fortunately, important recent work by Sadeh et al.²⁵ offers a resolution of this caveat and demonstrates that inhibition stabilization is best revealed through the suppression of activity selectively in inhibitory neurons over a broad region (>200 μm^2), while recording from the same neurons, to minimize the effects of competition between different inhibitory subtypes. Therefore, to more directly and conclusively test whether dorsal CA1 is an ISN, we built an optoelectrode with four optic fibers, each secured 50 μm above one shank of a 4-shank, 128-channel silicon probe.²⁶ This optrode design allowed us to simultaneously record from large populations of neurons while broadly illuminating the recorded region to affect a large population of cells (Figure 5). Additionally, we used infusions of AAV1-SIO-stGtACR2-fusionRed vector in Long Evans GAD-Cre rats to restrict opsin expression to the somata of GABAergic interneurons.^{27,28}

In these experiments ($n = 3$ rats, 5 sessions for CA1; $n = 2$ rats, 4 sessions in CA3b), we varied the intensity of light illumination over the course of recordings (Figure 5) to assess the effects of differing levels of perturbation.^{7,8,12} Remarkably, in CA1, at lower and intermediate light intensities, a large proportion of interneurons showed increases in firing, consistent with ISNs (Figures 5A–5C).²⁵ As the laser intensity was increased (up to 6 mW per optic fiber) a greater portion of interneurons showed suppressed firing in line with photoinhibition. This observation is also consistent with ISNs, for which although intermediate perturbations elicit paradoxical response dynamics, larger perturbations can overcome inhibitory stabilization and elicit non-ISN dynamics.^{12,25} In this range of laser intensities, CA1 pyramidal

neurons generally showed increased firing in response to photoinhibition of interneurons. This effect was also consistent with ISNs. In the CA3b experiments (Figures 5D–5F), a similar trend could be observed, though the effect appeared weaker and was only significant at intermediate settings of the laser intensity. This limited responsivity potentially indicates lower opsin expression or light delivery. Nevertheless, the observed neuronal responses remained consistent with ISNs: increased firing rates in interneurons at intermediate settings of laser intensity, with more cells showing decreased firing in response to photoinhibition at the higher laser intensities. We also performed similar experiments using an AAV1-CamKII α -stGtACR2-GFP vector to test the effect of large-scale photoinhibition that primarily targets excitatory neurons (Figure S6). These experiments produced results consistent with our previous ones: paradoxical firing rate increases in both CA1 and CA3, particularly among interneurons. Here, CA3 also showed a particularly strong paradoxical response among pyramidal neurons on the same shanks as the optical illumination.

Overall, these data demonstrate that both CA1 and CA3 networks exhibit inhibitory stabilization, with disinhibitory responses to photoinhibition elicited from both pyramidal cells and interneurons at intermediate laser intensities, while the stronger photoinhibition produced at higher light intensities results in decreased firing in an increasing number of inhibitory neurons.

Silencing CA3 results in disinhibition of CA1 interneurons

These optogenetic manipulations indicate that CA1 and CA3 networks are both inhibitory-stabilized and that neurons within each region produce paradoxical responses to optogenetic perturbations. We then examined whether these responses could affect cross-regional interactions, such as those between CA3 and CA1. Schaffer collaterals from CA3 provide one of the major synaptic inputs to CA1¹ and are considered to be important for the memory function of the hippocampus.^{29,30} We thus examined the effects of photoinhibition of CA3 on spiking activities of neurons in CA1. We infused AAV2-CamKII α -ArchT-GFP bilaterally into the dorsal CA3b subregion, which feeds into dorsal CA1. After a minimum of 2 weeks to allow for opsin expression, we performed a second surgery ($n = 4$ rats, 7 sessions, Figure 6) to implant bilateral optical fibers targeting CA3 and recording electrodes in dorsal CA1. In these experiments, we examined CA1 spike responses to optical perturbations in CA3 under urethane anesthesia. During the time windows of CA3 photoinhibition, CA1 pyr showed a heterogeneous response, with 75/303 neurons showing a significant increase in firing, while 129/303 neurons showed a significant decrease, with an overall small but significant increase in the mean firing rate. However, interneurons in CA1 showed a strong and significant increase in firing (Figure 6A) during CA3 photoinhibition. Of the 105 recorded int, 59 (56%) showed increases in firing, 20 (19%) showed decreases in firing, and 26 (25%) displayed no response to light stimulation.

In a second group of animals, we again delivered AAV2-CamKII α -ArchT-GFP bilaterally to dorsal CA3b, but we implanted bilateral CA3 optic fibers and CA1 electrodes chronically, to perform these experiments during normal rest in the home cage after recovery from surgery. Results from these experiments were consistent with those in the urethane-anesthetized

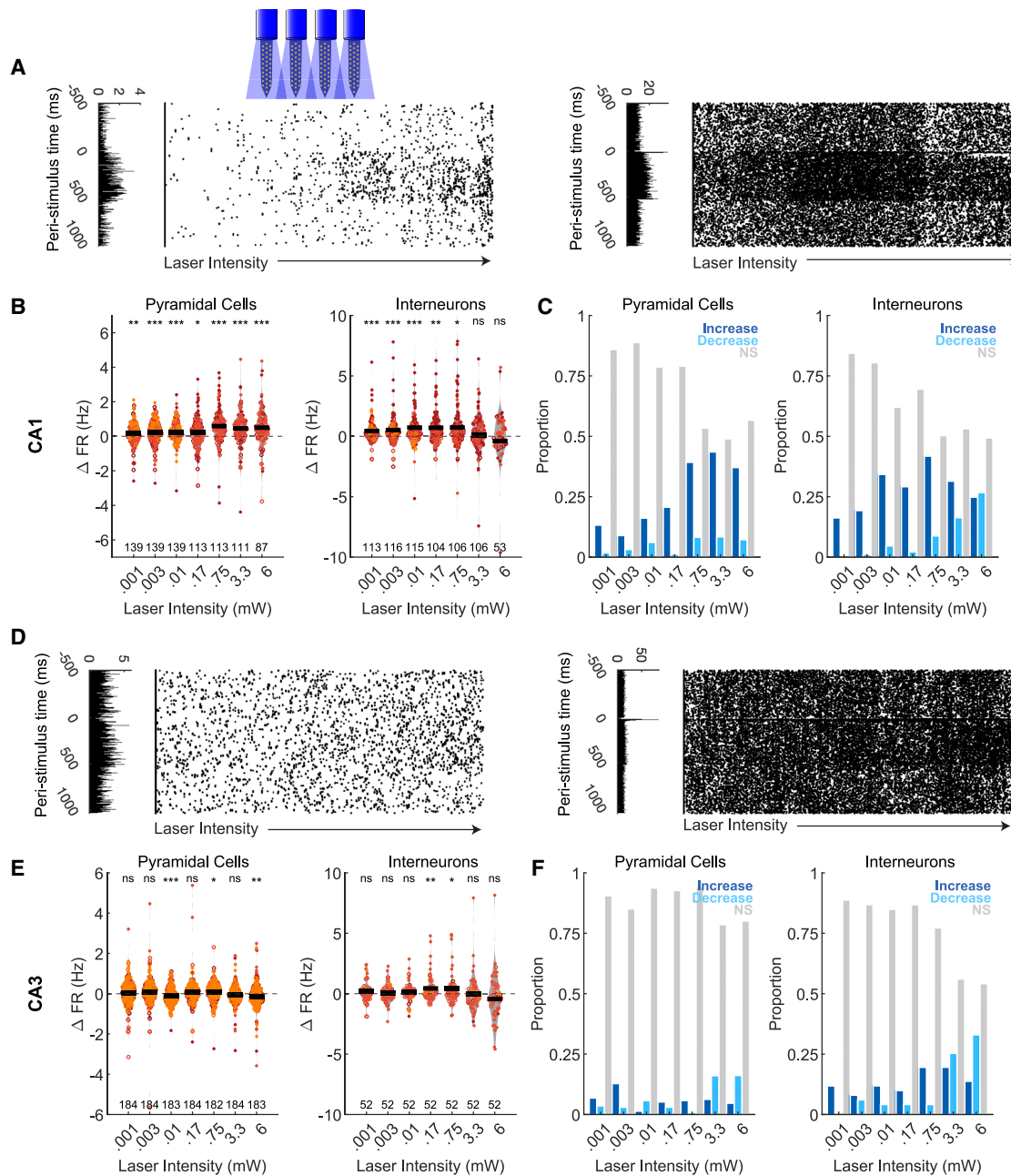


Figure 5. Responses to large-scale photoinhibition of interneurons in CA1 and CA3

Neuronal responses to broad multi-fiber photoinhibition in transgenic GAD-Cre rats expressing stGtACR2 in CA1 and CA3.

(A) Example raster responses of a pyramidal cell (left) and an interneuron (right) in CA1 across trials with varying intensities of illumination per fiber (from <math><0.001</math> to 6 mW) from a custom 4-fiber “Masmanidis” optrode. The pooled peri-event histograms are provided at the left of the rasters.

(B and C) (B) Population firing rate changes and (C) proportion plots for CA1 pyramidal cells (left) and interneurons (right) as a function of laser intensity. Individual cells overlaid on the population violin plots are colored according to animal, with the black horizontal line providing the group mean. Filled circles identify significantly modulated cells (binomial test, $\alpha = 0.01$). Numbers at the bottom of each panel provide the number of cells in each condition. Pyramidal cell firing rates broadly increased with photoinhibition. Interneuron firing rates also increased at low and intermediate light intensities, but at higher light intensities some cells showed decreased firing rates, with a non-significant net change in the overall population.

(D) Similar to (A), but for an example pyramidal cell (left) and interneuron (right) in CA3 as light intensity was increased from <math><0.001</math> to 6 mW per fiber.

(E and F) (E) Population firing rate changes and (F) proportion plots for CA3 pyramidal cells (left) and interneurons (right) as a function of laser intensity. Pyramidal cell responses in our experiments were muted, with little changes at most intensity levels. Interneurons, however, showed a small but significant increase in firing at intermediate illumination levels (e.g., laser intensity = 0.17 and 0.75 mW). * $p < 0.01$, ** $p < 0.001$, *** $p < 0.0001$, paired t test.

See Figure S4 and Tables S2 and S3 for comparisons with null baselines. See Figure S6 for results of broad multi-fiber illumination with the CamKII α -stGtACR2 opsin.

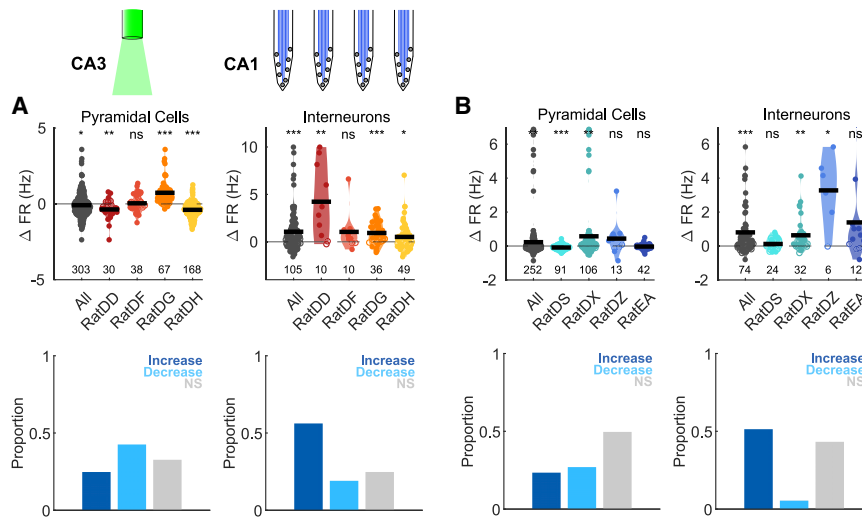


Figure 6. Responses of neurons in CA1 to photoinhibition of CA3 in anesthetized and awake animals

In these experiments, an optical fiber connected to a light source was implanted in the CA3 region of rats infused with CamKII α -ArchT in CA3, and recording electrodes were implanted in CA1.

(A) Pooled firing rate responses (top) and proportion plots (bottom) for pyramidal cells (left) and interneurons (right) recorded in each session as well as across all 4 sessions (1 session per animal), under urethane anesthesia. The numbers below each violin plot indicate the number of recorded cells for that animal, which were combined for “all.” The net response of pyramidal cells varied across sessions, with an overall mean = -0.09 Hz, with a smaller proportion of cells showing increased (75/303) compared with decreased (129/303) firing response (binomial test $p = 1.9104e-04$). CA1 interneurons generally showed increased

firing mean = 1.06 Hz, in response to CA3 photoinhibition, with a larger proportion of cells increasing rather than decreasing (binomial test $p = 1.2967e-05$).

(B) Same as in (A) but in awake animals during rest in a home cage. Similar observations were made for CA1 neurons in awake animals. Overall, pyramidal cell firing rates increased by mean = 0.23 Hz, with a mixed response (59 increase vs. 68 decrease, binomial $p = 0.4779$), while interneuron firing rates increased by 0.80 Hz during CA3 photoinhibition (with 38 increase vs. 4 decrease, binomial test $p = 5.6531e-08$). * $p < 0.01$, ** $p < 0.001$, *** $p < 0.0001$, paired t test.

See [Figure S4](#) and [Tables S2](#) and [S3](#) for comparisons with null baselines.

animals ([Figure 6B](#)). The overall population response of pyramidal cells showed a net neutral effect of stimulation because individual units responded heterogeneously, with similar proportions increasing (23%, 59/252) and decreasing (27%, 58/252) firing in response to upstream photoinhibition and 49% not responding. CA1 interneurons, on the other hand, displayed a significant mean firing increase. Of the 87 recorded CA1 int (4 rats, 8 sessions), 51% showed a paradoxical increase in firing, 5% decreased firing, and 43% had no response to light stimulation in CA3 ([Figure 6D](#)). Overall, these data demonstrate that silencing CA3 results in a net increase of interneuron firing activity in CA1.

An ISN model explains paradoxical firing responses to photoinhibition

The firing responses we uncovered in these optogenetics experiments are difficult to understand through intuition alone but appear to be consistent with the paradoxical effects produced by inhibitory stabilization. Furthermore, the effect of coupling two ISNs, one in CA1 and one in CA3, as indicated by our experimental results, has not been studied before (though see [Moore et al.⁶](#)). We therefore performed computational network modeling of a CA3 layer that projects onto a CA1 layer ([Figure 7](#)). Both cell layers were randomly connected; in CA3, as compared with CA1, we set the probability of recurrent excitatory connections higher but the individual synaptic weights lower to match the higher recurrence associated with CA3 while maintaining ISN behavior in both regions.^{12,25} We verified that these regions operate in an inhibitory-stabilized regime by clamping the inhibitory neurons and confirming that excitation saturates the network dynamics ([Figures S7A–S7D](#)). To model how CA3 manipulations affect CA1 networks, we modeled Schaffer collateral projections from CA3 and CA1 as directly synapsing both excitatory and inhibitory cells in CA1, consistent with experimental studies of this

neuroarchitecture.^{31–33} We first simulated the effects of separately manipulating either one of the two layers using optogenetic perturbations ([Figures 7A–7D](#)). Following [Sadeh et al.²⁵](#) the effects of photoinhibition/photoexcitation were modeled by adding a negative/positive constant to the background inputs into a varying proportion of cells and examining firing rate changes across both the directly perturbed and remaining neurons. We suppose that these parallel our experimental manipulations, where the proportion of directly to indirectly perturbed cells decreases with distance from the light source. Our simulations at a 25% perturbation level in CA1 showed decreased firing in directly perturbed excitatory and inhibitory neurons (E_{direct} and I_{direct} , respectively), whereas a subset of the non-perturbed cells in the network showed paradoxical firing rate increases (E and I), consistent with our CA1 optrode experiments ([Figure 7A](#); related to [Figure 1](#)). In simulations of similar manipulations in the CA3 pyramidal layer, we also observed decreased firing in neurons that directly receive photoinhibition ([Figure 7B](#); related to [Figure 2](#)). However, unperturbed neurons showed larger firing increases than in the CA1 simulations. This effect was likely due to the relatively higher recurrent connection probability in CA3 (see also [Figures S7E](#) and [S7F](#)). Simulations of photoexcitation of CA3 ([Figure 7C](#); related to [Figures 4D](#) and [4E](#)) in turn produced paradoxical firing rate decreases, even in directly perturbed cells. This effect was most evident in the excitatory population (e.g., note bimodality in responses of E_{direct} and $E_{indirect}$, cells at $Pert = 25\%$) similar to what we observed in the experiments. We confirmed that increasing the connection probability between excitatory neurons increases the paradoxical response in interneurons to direct photoinhibition ([Figure 7D](#)), as predicted, as well as the amount of off-target paradoxical responses to photoinhibition in indirectly perturbed cells ([Figures S7E](#) and [S7F](#)). Photoinhibition directed at a large subset of interneurons at varying levels of intensity (the background inputs) mimicked the results of

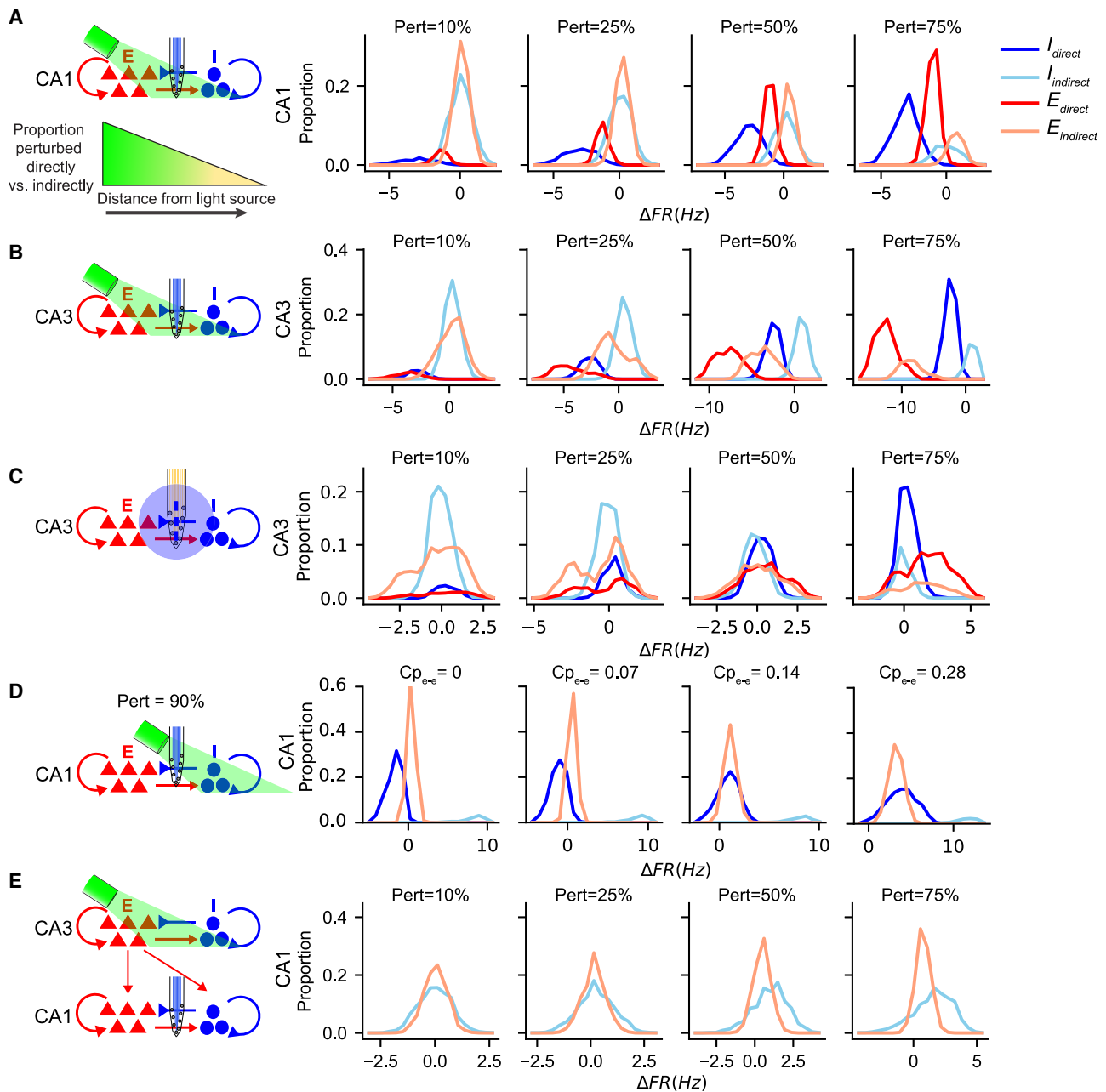


Figure 7. An inhibition-stabilized network model recapitulates the main experimental observations

(A–D) We performed simulations with a CA3–CA1 network in which both CA3 and CA1 were inhibition-stabilized. In (A) CA1 was photoinhibited, in (B) and (D) CA3 was photoinhibited, and in (C) CA3 was photostimulated (see additional simulations in Figure S7). In line with recent experimental observations, different subsets of both excitatory (E) and inhibitory (I) cells in our model were directly perturbed. Distribution of firing rate changes in four different subpopulations: directly perturbed excitatory and inhibitory neurons, E_{direct} and I_{direct} , respectively, and the indirectly perturbed excitatory and inhibitory neurons, $E_{indirect}$ and $I_{indirect}$, respectively. The columns show results for increasing the perturbation proportions (Pert%) of photoinhibited neurons (from left to right: 10%, 25%, 50%, and 75%) to examine different potential scenarios. As illustrated in the inset of (A), we suppose that the proportion of direct to indirect perturbations decreases with distance from the light source. (A) Photoinhibition in CA1 and (B) photoinhibition in CA3 reveal paradoxical firing rate increases in subsets of neurons. Note the generally wider distributions of changes across E and I in CA3 compared with CA1. Perturbation levels of 25% or 50% appear to provide a good match to experimental results from our optrode experiments. (C) Photostimulation in CA3, as in our μ LED experiments, at 10% or 25% perturbation levels produced paradoxical firing rate decreases, which was notable particularly in excitatory neurons (comparable to experimental observations in Figure 4D). (D) We simulated the effects of photoinhibition targeting specifically a large proportion (Pert = 90%) of interneurons in CA1, while we varied Cp_{e-e} . As the connection probability between E cells was increased, paradoxical firing rate increases were more readily observed in the directly photoinhibited I population (i.e., the two right panels).

(legend continued on next page)

the GAD-Cre multi-fiber experiments (Figures S7G and S7H; related to Figures 5A–5C). Lastly, we studied the effects of photo-inhibition of CA3 on CA1 firing patterns (Figure 7E; related to Figure 6) and found that it produced a shift in the distribution of firing rates in the CA1 network, consistent with our experimental observations. Both excitatory and inhibitory firing rates shifted toward increased activity, though this effect was more evident among inhibitory cells, similar to in our experimental data.

DISCUSSION

Our work demonstrates paradoxical effects from optogenetic perturbations in the hippocampus. Across multiple experiments, we found consistently that for some subsets of neurons, photo-inhibition produced paradoxical firing increases and photostimulation yielded paradoxical firing decreases. Although these results are unintuitive at first glance, we showed that our observations can be explained by dynamic models of a strongly recurrent excitatory network stabilized by inhibitory neurons. These models were first proposed by Tsodyks et al.¹² to explain theta-oscillation phase coherence between excitatory and inhibitory cell populations in the hippocampus. Since then, they have been used to explain receptive field properties, such as surround suppression in the visual cortex of rodents and cats.^{34,35} Evidence for ISNs, using optogenetic manipulations, similar to ours, has recently emerged for other brain regions, including the somatosensory, auditory, and visual cortices.^{7,8,13} Our investigation reveals that inhibitory stabilization is at work in the CA1 and CA3 regions of the hippocampus and, moreover, that ISN dynamics emerge in downstream regions when one region is perturbed. These findings further indicate that inhibitory stabilization is a common motif across circuits in both the archi-cortex and neocortex, despite apparently different neuronal architectures.

Inhibition stabilization has important implications for the computational capabilities of neuronal networks.¹³ For example, in the sensory system, models based on inhibitory stabilization demonstrate different regimes of computation, from supralinear summation of weak inputs to sublinear summation of strong inputs.³⁵ Our work (see also Table S4) implies that similar operations may also be at play in the hippocampus; supralinear summation during place cell activities during exploration can amplify weak spatial inputs,^{36,37} while sublinear summation during hippocampal sharp-wave ripples can provide competition between different ensembles of neurons.^{36,38} The strong recurrence associated with ISNs can also support associative learning³⁹ and sequence generation among competing neuronal assemblies.^{29,40} Inhibitory stabilization confers networks with such rich spatiotemporal structures for different computations while maintaining stability against unbounded amplification and epileptiform activities. For a network to operate in the ISN-regime, the main requirement is for strong recurrent connectivity between excitatory neurons that can amplify excitatory inputs and must be subsequently stabilized via inhibition.¹² This contrasts with weakly recurrent networks, where even though

excitation and inhibition may be coupled, neurons can show stable dynamics without a need for active inhibition. Our evidence for hippocampal ISNs and their predicate for active stabilization through inhibition can potentially account for the frequency of the hippocampus as a locus of epileptiform activity.⁴¹

Although off-target responses such as we report can take place even in non-ISNs, the key test of ISNs requires large-scale perturbations exclusive to the inhibitory cells. In particular, broad photoinhibition of inhibitory neurons in GAD-Cre rats expressing stGtACR2, as we performed here (Figure 5), provides a sensitive assay and unambiguous test of ISNs,^{7,25} as it can reveal the amplification of excitatory inputs in the ISN even with weak background activity. A surprising aspect of our findings is that this property holds not only for hippocampal region CA3, with well-known recurrent connectivity,^{1,39} but also for hippocampal region CA1 that has classically been considered to be largely feedforward.¹ Interestingly, though ISNs were introduced by Tsodyks et al.¹² explicitly to account for hippocampal dynamics, ours is the first study to test for hippocampal ISNs using optogenetics. We further modeled these dynamics in a spiking neuronal network that generated paradoxical firing increases in CA1 inhibitory cells during both photoinhibition of CA1 and during photoinhibition of CA3, which provides important excitatory input to CA1. The dynamics revealed by our experiments and modeling can provide an explanation for the inhibition-dominated dynamics in CA1 reported during sharp-wave ripples that originate in CA3.^{36,38} These experiment and modeling observations thus indicate that CA1, as well as CA3, features the strong excitatory-excitatory coupling that is a hallmark of ISNs.

Although this evidence for strong excitatory recurrence in CA1 is novel and surprising, it is also consistent with a number of other recent observations. First, while synaptic connections between CA1 pyramidal neurons are rare, there is compelling experimental evidence that they do in fact occur.^{42–45} In particular, Yang et al.⁴³ revealed strong evidence for intralaminar synaptic connections between CA1 cells, which were later shown to undergo long-term potentiation,⁴⁴ though not long-term depression, for reasons still unknown. Another recent study³⁷ also found evidence for CA1-CA1 synapses and suggested that these connections may play an important functional role in the formation and stabilization of place fields. Our network model took inspiration from these studies and showed that strong connections, at even relatively low connection probabilities, can produce ISN dynamics. However, excitatory-excitatory coupling in CA1 may also result from another source. There is evidence from *in vitro* and *in vivo* electrophysiology that CA1 pyramidal neurons are connected through axonal gap junctions.^{46,47} The spread of excitatory activity through direct electrical connections has been proposed as a way to account for fast hippocampal oscillations, such as those during sharp-wave ripples.^{48–50} Intracellular recordings from CA1 pyramidal cells also demonstrate an abundance of spikelets that appear to be consistent with axo-axonically transmitted signals between such neurons.^{51,52} A third, more speculative, possibility is that complementary connections between CA1 and the subiculum,^{53–55} or reentry loops through the entorhinal

(E) Photoinhibition in CA3 produces paradoxical firing rate increases in CA1 neurons. The firing rate increases are most evident in the inhibitory subpopulation, similar to experimental results in Figure 6. See also Table S4.

cortex,^{54,56} could effectively push dynamics of the larger network into an ISN regime. More research is needed to better understand how excitability passes through hippocampal neural architecture. Nevertheless, our modeling and experimental observations combined are consistent with experimental evidence for a CA1 role in generating coherent waves of excitation when inhibition is temporarily decreased,^{57,58} including in the absence of CA3 input.⁵⁸

Our results also highlight that the complexities of circuit interactions means that neurons do not respond to optogenetic manipulations in straightforward ways. Local perturbations generated heterogeneous responses in both pyramidal cells and interneurons, even at the site of illumination. The proportion of interneurons with increased firing increased as a function of distance from the site of illumination and was dependent on the spatial spread and intensity of illumination. However, even with very focal light delivered with μ LEDs, we observed cells that increased firing during photoinhibition and ones that decreased firing during photoinhibition. Such paradoxical responses have been reported in previous studies.^{19,59,60} In our investigation, such responses were more prevalent in CA3 than in CA1, though still evident in both regions, indicating that connectivity patterns play an important role in how manipulations percolate through a particular brain circuit. Additionally, we note that the proportion of paradoxically responding cells increased as a function of distance from the site of illumination. As many studies that employ optogenetic tools do not examine simultaneous unit responses, particularly on electrodes not directly attached to the optical fiber used to deliver light, it must be considered that the off-target effects of these perturbations play an important role in generating the brain response to optogenetic manipulations (see also Otchy et al.⁶¹). Together, these data indicate that off-target responses to focal perturbations may occur to a greater degree in some circuits than others, even among ISNs. Such differences likely reflect aspects of the local circuitry, including differences in connection probabilities, which can provide insights into how networks with varying connectivity respond to acute perturbations of excitatory-inhibitory balance.

An additional important observation in our study is that paradoxical effects can emerge downstream from the manipulated region. During windows of CA3 photoinhibition, we observed increased firing in CA1, particularly among interneurons. Our model demonstrated that these dynamics could emerge when excitatory input to CA1 interneurons is diminished. Indeed, there is extensive evidence that CA1 interneurons receive direct excitatory inputs from area CA3, thus providing feedforward inhibition in the local network.^{31,33,62–66} This feedforward inhibition may be functionally relevant for limiting the window of synaptic integration of CA3 inputs,^{32,63} providing temporal windows for neuronal computations in the hippocampus⁶⁷ and the propagation of information at specific oscillation frequencies.³³ Importantly, similar feedforward connectivity patterns are evident in other regions throughout the brain.⁶ Thus, paradoxical effects are likely in downstream targets of most brain circuits, especially if those targets feature strong recurrent connections—a frequent motif in the brain.^{7,8} Given that the number of downstream regions that are recorded from are typically limited, our findings add to the body of work signaling that care must be taken in evaluating results from optogenetic and other perturbation studies on off-target activity.^{68–70}

STAR★METHODS

Detailed methods are provided in the online version of this paper and include the following:

- KEY RESOURCES TABLE
- RESOURCE AVAILABILITY
 - Lead Contact
 - Materials availability
 - Data and code availability
- EXPERIMENTAL MODEL AND SUBJECT DETAILS
- METHOD DETAILS
 - Fiber-based optoelectronic design ('optrodes')
 - Virus Surgery
 - Anesthetized Recordings
 - Chronic Recordings
 - Data acquisition
 - Histology
 - Spiking network models
- QUANTIFICATION AND STATISTICAL ANALYSIS
 - Data processing and cell classification
 - Cell response statistics

SUPPLEMENTAL INFORMATION

Supplemental information can be found online at <https://doi.org/10.1016/j.cub.2023.03.032>.

ACKNOWLEDGMENTS

This work was supported by the German Federal Ministry of Education and Research (BMBF) grant 01GQ1506 (to S.C.), German Research Foundation (DFG) grant 122679504–SFB 874, B2 (to S.C.), and from the National Institutes of Health, NIMH R01MH109170, NINDS R21NS088798, and R01NS115233 (to K.D.). The high-performance computing facilities used for the simulations of this project were provided by the Paderborn Center for Parallel Computing, PC² (to M.M.N.).

We thank Joseph Watkins, David Lyttle, and Yunchang Zhang for assistance on experiments and analyses, and Gideon Rothschild, Rachel Wahlberg, Nat Kinsky, and Pho Hale for comments on the manuscript.

AUTHOR CONTRIBUTIONS

L.W.d.J. performed experiments and analyses; L.W.d.J. and K.D. designed the experiments; M.M.N. developed and simulated the model and analyzed results from the model; E.Y. contributed μ LED optrodes; S.C. supervised the modeling; K.D. wrote the manuscript, with comments and edits from all authors.

DECLARATION OF INTERESTS

E.Y. is a co-founder of NeuroLight Technologies, a for-profit manufacturer of μ LED optoelectrodes.

INCLUSION AND DIVERSITY

We support inclusive, diverse, and equitable conduct of research.

Received: August 19, 2022

Revised: February 22, 2023

Accepted: March 10, 2023

Published: April 5, 2023

REFERENCES

- Amaral, D.G., and Lavenex, P. (2006). Hippocampal neuroanatomy. In *The Hippocampus*, C.A. Book, R.G. Morris, D.G. Amaral, and J. O'Keefe, eds. (Oxford University Press), pp. 4–33.
- Shepherd, G. (2003). *Synaptic Organization of the Brain, 34d Edition* (Oxford University Press).
- Klausberger, T., and Somogyi, P. (2008). Neuronal diversity and temporal dynamics: the unity of hippocampal circuit operations. *Science* 321, 53–57. <https://doi.org/10.1126/science.1149381>.
- Fenno, L., Yizhar, O., and Deisseroth, K. (2011). The development and application of optogenetics. *Annu. Rev. Neurosci.* 34, 389–412. <https://doi.org/10.1146/annurev-neuro-061010-113817>.
- Atallah, B.V., Bruns, W., Carandini, M., and Scanziani, M. (2012). Parvalbumin-expressing interneurons linearly transform cortical responses to visual stimuli. *Neuron* 73, 159–170. <https://doi.org/10.1016/j.neuron.2011.12.013>.
- Moore, A.K., Weible, A.P., Balmer, T.S., Trussell, L.O., and Wehr, M. (2018). Rapid rebalancing of excitation and inhibition by cortical circuitry. *Neuron* 97, 1341.e6–1355.e6. <https://doi.org/10.1016/j.neuron.2018.01.045>.
- Sanzeni, A., Akitake, B., Goldbach, H.C., Leedy, C.E., Brunel, N., and Histed, M.H. (2020). Inhibition stabilization is a widespread property of cortical networks. *eLife* 9, e54875. <https://doi.org/10.7554/eLife.54875>.
- Li, N., Chen, S., Guo, Z.V., Chen, H., Huo, Y., Inagaki, H.K., Chen, G., Davis, C., Hansel, D., Guo, C., et al. (2019). Spatiotemporal constraints on optogenetic inactivation in cortical circuits. *eLife* 8, e48622. <https://doi.org/10.7554/eLife.48622>.
- Phillips, E.A., and Hasenstaub, A.R. (2016). Asymmetric effects of activating and inactivating cortical interneurons. *eLife* 5, e18383. <https://doi.org/10.7554/eLife.18383>.
- Mahrach, A., Chen, G., Li, N., van Vreeswijk, C., and Hansel, D. (2020). Mechanisms underlying the response of mouse cortical networks to optogenetic manipulation. *eLife* 9, e49967. <https://doi.org/10.7554/eLife.49967>.
- Robinson, N.T.M., Descamps, L.A.L., Russell, L.E., Buchholz, M.O., Bicknell, B.A., Antonov, G.K., Lau, J.Y.N., Nutbrown, R., Schmidt-Hieber, C., and Häusser, M. (2020). Targeted Activation of Hippocampal Place Cells Drives Memory-Guided Spatial Behavior. *Cell* 183, 2041–2042. <https://doi.org/10.1016/j.cell.2020.12.010>.
- Tsodyks, M.V., Skaggs, W.E., Sejnowski, T.J., and McNaughton, B.L. (1997). Paradoxical effects of external modulation of inhibitory interneurons. *J. Neurosci.* 17, 4382–4388.
- Sadeh, S., and Clopath, C. (2021). Inhibitory stabilization and cortical computation. *Nat. Rev. Neurosci.* 22, 21–37. <https://doi.org/10.1038/s41583-020-00390-z>.
- Royer, S., Zemelman, B.V., Barbic, M., Losonczy, A., Buzsáki, G., and Magee, J.C. (2010). Multi-array silicon probes with integrated optical fibers: light-assisted perturbation and recording of local neural circuits in the behaving animal. *Eur. J. Neurosci.* 31, 2279–2291. <https://doi.org/10.1111/j.1460-9568.2010.07250.x>.
- Bermudez Contreras, E.J., Schjettan, A.G., Muhammad, A., Bartho, P., McNaughton, B.L., Kolb, B., Gruber, A.J., and Luczak, A. (2013). Formation and reverberation of sequential neural activity patterns evoked by sensory stimulation are enhanced during cortical desynchronization. *Neuron* 79, 555–566. <https://doi.org/10.1016/j.neuron.2013.06.013>.
- Clement, E.A., Richard, A., Thwaites, M., Ailon, J., Peters, S., and Dickson, C.T. (2008). Cyclic and sleep-like spontaneous alternations of brain state under urethane anaesthesia. *PLoS One* 3, e2004. <https://doi.org/10.1371/journal.pone.0002004>.
- Hahn, T.T., McFarland, J.M., Berberich, S., Sakmann, B., and Mehta, M.R. (2012). Spontaneous persistent activity in entorhinal cortex modulates cortico-hippocampal interaction in vivo. *Nat. Neurosci.* 15, 1531–1538. <https://doi.org/10.1038/nn.3236>.
- Nathanson, J.L., Yanagawa, Y., Obata, K., and Callaway, E.M. (2009). Preferential labeling of inhibitory and excitatory cortical neurons by endogenous tropism of adeno-associated virus and lentivirus vectors. *Neuroscience* 161, 441–450. <https://doi.org/10.1016/j.neuroscience.2009.03.032>.
- Schoenenberger, P., O'Neill, J., and Csicsvari, J. (2016). Activity-dependent plasticity of hippocampal place maps. *Nat. Commun.* 7, 11824. <https://doi.org/10.1038/ncomms11824>.
- Mahn, M., Prigge, M., Ron, S., Levy, R., and Yizhar, O. (2016). Biophysical constraints of optogenetic inhibition at presynaptic terminals. *Nat. Neurosci.* 19, 554–556. <https://doi.org/10.1038/nn.4266>.
- El-Gaby, M., Zhang, Y., Wolf, K., Schwiening, C.J., Paulsen, O., and Shipton, O.A. (2016). Archaelhodopsin selectively and reversibly silences synaptic transmission through altered pH. *Cell Rep.* 16, 2259–2268. <https://doi.org/10.1016/j.celrep.2016.07.057>.
- Wu, F., Stark, E., Ku, P.C., Wise, K.D., Buzsáki, G., and Yoon, E. (2015). Monolithically integrated muLEDs on silicon neural probes for high-resolution optogenetic studies in behaving animals. *Neuron* 88, 1136–1148. <https://doi.org/10.1016/j.neuron.2015.10.032>.
- Lin, J.Y., Lin, M.Z., Steinbach, P., and Tsien, R.Y. (2009). Characterization of engineered channelrhodopsin variants with improved properties and kinetics. *Biophys. J.* 96, 1803–1814. <https://doi.org/10.1016/j.bpj.2008.11.034>.
- Litwin-Kumar, A., Rosenbaum, R., and Doiron, B. (2016). Inhibitory stabilization and visual coding in cortical circuits with multiple interneuron subtypes. *J. Neurophysiol.* 115, 1399–1409. <https://doi.org/10.1152/jn.00732.2015>.
- Sadeh, S., Silver, R.A., Mrcic-Flogel, T.D., and Muir, D.R. (2017). Assessing the role of inhibition in stabilizing neocortical networks requires large-scale perturbation of the inhibitory population. *J. Neurosci.* 37, 12050–12067. <https://doi.org/10.1523/JNEUROSCI.0963-17.2017>.
- Yang, L., Lee, K., Villagrancia, J., and Masmanidis, S.C. (2020). Open source silicon microprobes for high throughput neural recording. *J. Neural Eng.* 17, 016036. <https://doi.org/10.1088/1741-2552/ab581a>.
- Sharpe, M.J., Marchant, N.J., Whitaker, L.R., Richie, C.T., Zhang, Y.J., Campbell, E.J., Koivula, P.P., Necarsulmer, J.C., Mejias-Aponte, C., Morales, M., et al. (2017). Lateral hypothalamic GABAergic neurons encode reward predictions that are relayed to the ventral tegmental area to regulate learning. *Curr. Biol.* 27, 2089.e5–2100.e5. <https://doi.org/10.1016/j.cub.2017.06.024>.
- Mahn, M., Gibor, L., Patil, P., Cohen-Kashi Malina, K., Oring, S., Printz, Y., Levy, R., Lampl, I., and Yizhar, O. (2018). High-efficiency optogenetic silencing with soma-targeted anion-conducting channelrhodopsins. *Nat. Commun.* 9, 4125. <https://doi.org/10.1038/s41467-018-06511-8>.
- Cheng, S. (2013). The CRISP theory of hippocampal function in episodic memory. *Front. Neural Circuits* 7, 88. <https://doi.org/10.3389/fncir.2013.00088>.
- Rolls, E.T. (2018). The storage and recall of memories in the hippocampal-cortical system. *Cell Tissue Res.* 373, 577–604. <https://doi.org/10.1007/s00441-017-2744-3>.
- Milstein, A.D., Bloss, E.B., Apostolides, P.F., Vaidya, S.P., Dilly, G.A., Zemelman, B.V., and Magee, J.C. (2015). Inhibitory gating of input comparison in the CA1 microcircuit. *Neuron* 87, 1274–1289. <https://doi.org/10.1016/j.neuron.2015.08.025>.
- Pouille, F., and Scanziani, M. (2004). Routing of spike series by dynamic circuits in the hippocampus. *Nature* 429, 717–723.
- Zemankovics, R., Veres, J.M., Oren, I., and Hájos, N. (2013). Feedforward inhibition underlies the propagation of cholinergically induced gamma oscillations from hippocampal CA3 to CA1. *J. Neurosci.* 33, 12337–12351. <https://doi.org/10.1523/JNEUROSCI.3680-12.2013>.
- Ozeki, H., Finn, I.M., Schaffer, E.S., Miller, K.D., and Ferster, D. (2009). Inhibitory stabilization of the cortical network underlies visual surround suppression. *Neuron* 62, 578–592. <https://doi.org/10.1016/j.neuron.2009.03.028>.

35. Rubin, D.B., Van Hooser, S.D., and Miller, K.D. (2015). The stabilized supralinear network: a unifying circuit motif underlying multi-input integration in sensory cortex. *Neuron* 85, 402–417. <https://doi.org/10.1016/j.neuron.2014.12.026>.
36. Valero, M., Zutshi, I., Yoon, E., and Buzsáki, G. (2022). Probing subthreshold dynamics of hippocampal neurons by pulsed optogenetics. *Science* 375, 570–574. <https://doi.org/10.1126/science.abm1891>.
37. Geiller, T., Sadeh, S., Rolotti, S.V., Blockus, H., Vancura, B., Negrean, A., Murray, A.J., Rózsa, B., Polleux, F., Clopath, C., and Losonczy, A. (2022). Local circuit amplification of spatial selectivity in the hippocampus. *Nature* 601, 105–109. <https://doi.org/10.1038/s41586-021-04169-9>.
38. Noguchi, A., Huszár, R., Morikawa, S., Buzsáki, G., and Ikegaya, Y. (2022). Inhibition allocates spikes during hippocampal ripples. *Nat. Commun.* 13, 1280. <https://doi.org/10.1038/s41467-022-28890-9>.
39. Le Duigou, C., Simonnet, J., Teleńczuk, M.T., Fricker, D., and Miles, R. (2014). Recurrent synapses and circuits in the CA3 region of the hippocampus: an associative network. *Front. Cell. Neurosci.* 7, 262. <https://doi.org/10.3389/fncel.2013.00262>.
40. Rajan, K., Harvey, C.D., and Tank, D.W. (2016). Recurrent network models of sequence generation and memory. *Neuron* 90, 128–142. <https://doi.org/10.1016/j.neuron.2016.02.009>.
41. Avoli, M. (2007). The epileptic hippocampus revisited: back to the future. *Epilepsy Curr.* 7, 116–118. <https://doi.org/10.1111/j.1535-7511.2007.00194.x>.
42. Deuchars, J., and Thomson, A.M. (1996). CA1 pyramid-pyramid connections in rat hippocampus in vitro: dual intracellular recordings with biocytin filling. *Neuroscience* 74, 1009–1018. [https://doi.org/10.1016/0306-4522\(96\)00251-5](https://doi.org/10.1016/0306-4522(96)00251-5).
43. Yang, S., Yang, S., Moreira, T., Hoffman, G., Carlson, G.C., Bender, K.J., Alger, B.E., and Tang, C.M. (2014). Interlamellar CA1 network in the hippocampus. *Proc. Natl. Acad. Sci. USA* 111, 12919–12924. <https://doi.org/10.1073/pnas.1405468111>.
44. Sun, D.G., Kang, H., Tetteh, H., Su, J., Lee, J., Park, S.W., He, J., Jo, J., Yang, S., and Yang, S. (2018). Long term potentiation, but not depression, in interlamellar hippocampus CA1. *Sci. Rep.* 8, 5187. <https://doi.org/10.1038/s41598-018-23369-4>.
45. Alger, B.E., and Teyler, T.J. (1977). A monosynaptic fiber track studied in vitro: evidence of a hippocampal CA1 associational system? *Brain Res. Bull.* 2, 355–365. [https://doi.org/10.1016/0361-9230\(77\)90069-7](https://doi.org/10.1016/0361-9230(77)90069-7).
46. Mercer, A., Bannister, A.P., and Thomson, A.M. (2006). Electrical coupling between pyramidal cells in adult cortical regions. *Brain Cell Biol.* 35, 13–27. <https://doi.org/10.1007/s11068-006-9005-9>.
47. Schmitz, D., Schuchmann, S., Fisahn, A., Draguhn, A., Buhl, E.H., Petrasch-Parwez, E., Dermietzel, R., Heinemann, U., and Traub, R.D. (2001). Axo-axonal coupling, a novel mechanism for ultrafast neuronal communication. *Neuron* 31, 831–840. [https://doi.org/10.1016/s0896-6273\(01\)00410-x](https://doi.org/10.1016/s0896-6273(01)00410-x).
48. Draguhn, A., Traub, R.D., Schmitz, D., and Jefferys, J.G. (1998). Electrical coupling underlies high-frequency oscillations in the hippocampus in vitro. *Nature* 394, 189–192. <https://doi.org/10.1038/28184>.
49. Traub, R.D., and Bibbig, A. (2000). A model of high-frequency ripples in the hippocampus based on synaptic coupling plus axon-axon gap junctions between pyramidal neurons. *J. Neurosci.* 20, 2086–2093.
50. Traub, R.D., Draguhn, A., Whittington, M.A., Baldeweg, T., Bibbig, A., Buhl, E.H., and Schmitz, D. (2002). Axonal gap junctions between principal neurons: a novel source of network oscillations, and perhaps epileptogenesis. *Rev. Neurosci.* 13, 1–30.
51. Epsztein, J., Lee, A.K., Chorev, E., and Brecht, M. (2010). Impact of spikelets on hippocampal CA1 pyramidal cell activity during spatial exploration. *Science* 327, 474–477. <https://doi.org/10.1126/science.1182773>.
52. Chorev, E., and Brecht, M. (2012). In vivo dual intra- and extracellular recordings suggest bidirectional coupling between CA1 pyramidal neurons. *J. Neurophysiol.* 108, 1584–1593. <https://doi.org/10.1152/jn.01115.2011>.
53. Sun, Y., Jin, S., Lin, X., Chen, L., Qiao, X., Jiang, L., Zhou, P., Johnston, K.G., Golshani, P., Nie, Q., et al. (2019). CA1-projecting subiculum neurons facilitate object-place learning. *Nat. Neurosci.* 22, 1857–1870. <https://doi.org/10.1038/s41593-019-0496-y>.
54. Sun, Y., Nitz, D.A., Holmes, T.C., and Xu, X. (2018). Opposing and complementary topographic connectivity gradients revealed by quantitative analysis of canonical and noncanonical hippocampal CA1 inputs. *eNeuro* 5, ENEURO.0322-17.2018. <https://doi.org/10.1523/ENEURO.0322-17.2018>.
55. Sun, Y., Nguyen, A.Q., Nguyen, J.P., Le, L., Saur, D., Choi, J., Callaway, E.M., and Xu, X. (2014). Cell-type-specific circuit connectivity of hippocampal CA1 revealed through Cre-dependent rabies tracing. *Cell Rep.* 7, 269–280. <https://doi.org/10.1016/j.celrep.2014.02.030>.
56. Tamamaki, N., and Nojyo, Y. (1995). Preservation of topography in the connections between the subiculum, field CA1, and the entorhinal cortex in rats. *J. Comp. Neurol.* 353, 379–390. <https://doi.org/10.1002/cne.903530306>.
57. Hulse, B.K., Moreaux, L.C., Lubenov, E.V., and Siapas, A.G. (2016). Membrane potential dynamics of CA1 pyramidal neurons during hippocampal ripples in awake mice. *Neuron* 89, 800–813. <https://doi.org/10.1016/j.neuron.2016.01.014>.
58. Maier, N., Tejero-Cantero, A., Dornn, A.L., Winterer, J., Beed, P.S., Morris, G., Kempster, R., Poulet, J.F., Leibold, C., and Schmitz, D. (2011). Coherent phasic excitation during hippocampal ripples. *Neuron* 72, 137–152. <https://doi.org/10.1016/j.neuron.2011.08.016>.
59. Do-Monte, F.H., Quiñones-Laracuente, K., and Quirk, G.J. (2015). A temporal shift in the circuits mediating retrieval of fear memory. *Nature* 519, 460–463. <https://doi.org/10.1038/nature14030>.
60. Han, X., Chow, B.Y., Zhou, H., Klapoetke, N.C., Chuong, A., Rajimehr, R., Yang, A., Baratta, M.V., Winkle, J., Desimone, R., and Boyden, E.S. (2011). A high-light sensitivity optical neural silencer: development and application to optogenetic control of non-human primate cortex. *Front. Syst. Neurosci.* 5, 18. <https://doi.org/10.3389/fnsys.2011.00018>.
61. Otchy, T.M., Wolff, S.B., Rhee, J.Y., Pehlevan, C., Kawai, R., Kempf, A., Gobes, S.M., and Ölveczky, B.P. (2015). Acute off-target effects of neural circuit manipulations. *Nature* 528, 358–363. <https://doi.org/10.1038/nature16442>.
62. Alger, B.E., and Nicoll, R.A. (1982). Feed-forward dendritic inhibition in rat hippocampal pyramidal cells studied in vitro. *J. Physiol.* 328, 105–123. <https://doi.org/10.1113/jphysiol.1982.sp014255>.
63. Pouille, F., Marin-Burgin, A., Adesnik, H., Atallah, B.V., and Scanziani, M. (2009). Input normalization by global feedforward inhibition expands cortical dynamic range. *Nat. Neurosci.* 12, 1577–1585. <https://doi.org/10.1038/nn.2441>.
64. Gulyás, A.I., Megias, M., Emri, Z., and Freund, T.F. (1999). Total number and ratio of excitatory and inhibitory synapses converging onto single interneurons of different types in the CA1 area of the rat hippocampus. *J. Neurosci.* 19, 10082–10097.
65. Maccaferri, G., and Dingledine, R. (2002). Control of feedforward dendritic inhibition by NMDA receptor-dependent spike timing in hippocampal interneurons. *J. Neurosci.* 22, 5462–5472.
66. Wierenga, C.J., and Wadman, W.J. (2003). Excitatory inputs to CA1 interneurons show selective synaptic dynamics. *J. Neurophysiol.* 90, 811–821. <https://doi.org/10.1152/jn.00865.2002>.
67. McKenzie, S. (2018). Inhibition shapes the organization of hippocampal representations. *Hippocampus* 28, 659–671. <https://doi.org/10.1002/hipo.22803>.
68. Wolff, S.B., and Ölveczky, B.P. (2018). The promise and perils of causal circuit manipulations. *Curr. Opin. Neurobiol.* 49, 84–94. <https://doi.org/10.1016/j.conb.2018.01.004>.
69. Jazayeri, M., and Afraz, A. (2017). Navigating the neural space in search of the neural code. *Neuron* 93, 1003–1014. <https://doi.org/10.1016/j.neuron.2017.02.019>.

70. Wiegert, J.S., Mahn, M., Prigge, M., Printz, Y., and Yizhar, O. (2017). Silencing neurons: tools, applications, and experimental constraints. *Neuron* 95, 504–529. <https://doi.org/10.1016/j.neuron.2017.06.050>.
71. Paxinos, G., and Watson, C. (2007). *The Rat Brain in Stereotaxic Coordinates, Sixth Edition* (Academic Press/Elsevier).
72. Chung, J., Sharif, F., Jung, D., Kim, S., and Royer, S. (2017). Micro-drive and headgear for chronic implant and recovery of optoelectronic probes. *Sci. Rep.* 7, 2773. <https://doi.org/10.1038/s41598-017-03340-5>.
73. Siegle, J.H., López, A.C., Patel, Y.A., Abramov, K., Ohayon, S., and Voigts, J. (2017). Open Ephys: an open-source, plugin-based platform for multi-channel electrophysiology. *J. Neural Eng.* 14, 045003. <https://doi.org/10.1088/1741-2552/aa5eea>.
74. Kinsky, N.R., Vöröslakos, M., Ruiz, J.R.L., Watkins de Jong, L., Slager, N., McKenzie, S., Yoon, E., and Diba, K. (2023). Simultaneous electrophysiology and optogenetic perturbation of the same neurons in chronically implanted animals using μ LED silicon probes. Preprint at bioRxiv. <https://doi.org/10.1101/2023.02.05.527184>.
75. Vöröslakos, M., Miyawaki, H., Royer, S., Diba, K., Yoon, E., Petersen, P.C., and Buzsáki, G. (2021). 3D-printed recoverable microdrive and base plate system for rodent electrophysiology. *Bio Protoc.* 11, e4137. <https://doi.org/10.21769/BioProtoc.4137>.
76. Gewaltig, M.O., and Diesmann, M. (2007). NEST (neural simulation tool). *Scholarpedia* 2, 1430.
77. Brette, R., and Gerstner, W. (2005). Adaptive exponential integrate-and-fire model as an effective description of neuronal activity. *J. Neurophysiol.* 94, 3637–3642. <https://doi.org/10.1152/jn.00686.2005>.
78. Rossant, C., Kadir, S.N., Goodman, D.F.M., Schulman, J., Hunter, M.L.D., Saleem, A.B., Grosmark, A., Belluscio, M., Denfield, G.H., Ecker, A.S., et al. (2016). Spike sorting for large, dense electrode arrays. *Nat. Neurosci.* 19, 634–641. <https://doi.org/10.1038/nn.4268>.
79. Hazan, L., Zugaro, M., and Buzsáki, G. (2006). Klusters, NeuroScope, NDManager: a free software suite for neurophysiological data processing and visualization. *J. Neurosci. Methods* 155, 207–216.
80. Mizuseki, K., Sirota, A., Pastalkova, E., and Buzsáki, G. (2009). Theta oscillations provide temporal windows for local circuit computation in the entorhinal-hippocampal loop. *Neuron* 64, 267–280. <https://doi.org/10.1016/j.neuron.2009.08.037>.
81. Royer, S., Zemelman, B.V., Losonczy, A., Kim, J., Chance, F., Magee, J.C., and Buzsáki, G. (2012). Control of timing, rate and bursts of hippocampal place cells by dendritic and somatic inhibition. *Nat. Neurosci.* 15, 769–775. <https://doi.org/10.1038/nn.3077>.

STAR★METHODS

KEY RESOURCES TABLE

REAGENT or RESOURCE	SOURCE	IDENTIFIER
Chemicals, peptides, and recombinant proteins		
AAV2/CamKII α -ARCT-GFP	UNC Vector Core	Addgene Plasmid #99039
AAV5/hSyn-oCHIEF-tdTomato	Duke Vector Core	Addgene Plasmid #50977
AAV1/CamKII α -stGtACR2-fusionRed	Ofer Yizhar via Addgene Viral Prep	Addgene Plasmid #105669
AAV1/hSyn-SIO-stGtACR2-FusionRed	Ofer Yizhar via Addgene Viral Prep	Addgene viral prep #105677
Experimental models: Organisms/strains		
LE-Tg(Gad1-iCre)3Otc rats	Rat Resource and Research Center	RRID: RRRRC_00751
Software and algorithms		
MATLAB code for generating figures	This paper	https://doi.org/10.5281/zenodo.7668352
Model code for generating simulations	This paper	https://doi.org/10.5281/zenodo.7669054
Other		
μ LED optoelectrodes	MINT Neuronex Technology Hub	https://mint.engin.umich.edu/

RESOURCE AVAILABILITY

Lead Contact

Requests for further information or data produced and analyzed in this study should be directed to and will be fulfilled by the lead contact, Kamran Diba (kdiba@umich.edu)

Materials availability

This study did not generate new unique reagents.

Data and code availability

Data reported in this paper will be shared by the lead contact upon request.

The analysis code is available at <https://github.com/diba-lab/LaurelWatkinsManuscript>. The modeling code is available at <https://github.com/sencheng/isn-model>. DOIs are listed in the key resources table.

Any additional information required to reanalyze the data reported in this paper is available from the lead contact upon request.

EXPERIMENTAL MODEL AND SUBJECT DETAILS

Subjects for the majority of experiments were wild type (WT) male Long-Evans rats (300-400g) obtained from Envigo (Haslett, MI) or Charles River Labs (Mattawan, MI). Prior to and following experiments, animals were housed in Double-Decker cages (Tecniplast) under 12 h light/dark cycles in a dedicated room adjoining the lab. Animal care was provided by Animal Care Program at the University of Wisconsin-Milwaukee and the Unit for Laboratory Animal Medicine at the University of Michigan. Male transgenic rats (LE-Tg(Gad1-iCre)3Otc expressing the Cre recombinase in cells where GAD1 promoter is active) were originally obtained through the Rat Resource and Research Center (RRID: RRRRC_00751) and were bred with female WT Long-Evans rats. The breeding colony was maintained by the Unit for Laboratory Animal Medicine at the University of Michigan and genotyped by Transnetyx Genetics Services. Both male and female transgenic animals (300-400g) were used in experiments localizing stGtACR2 opsin to inhibitory cells and no sex differences were evident. All experiments were approved by the Institutional Animal Care and Use Committees (IACUC) at the University of Wisconsin—Milwaukee and the University of Michigan and followed the US National Institutes of Health animal use guidelines.

METHOD DETAILS

Fiber-based optoelectronic design ('optrodes')

Optrodes were built according to previous design.¹⁴ Briefly, 125 μ m multimodal fibers were either cleaved to create a perfectly flat end-face or cone-etched for easier penetration using hydrofluoric acid. Using a micromanipulator, the optic fiber was placed on a shank of a silicon probe (Buz32 or Buz64; Neuronexus Inc, or Masmanidis 128K²⁶) with the fiber tip 50 μ m above the highest electrode site (Masmanidis 128K) or at a slight angle ($\sim 15^\circ$) 400 μ m above the highest electrode (Buz32 or Buz64). The fiber was secured to the bonding area

of the probe using either epoxy (Resinlab EP965 Black, Masmanidis 128K) or UV light-curable glue followed by dental acrylic (Buz32 or Buz64). This process was repeated, so that two (Buz32 or Buz64) or four (Masmanidis 128K) shanks were equipped with optic fibers.

Virus Surgery

Animals were anesthetized with isoflurane (induction at 5%, maintained at 1-2% during surgery) and placed in ear bars on a stereotaxic stage. Rats were placed on a heating pad to prevent loss of body temperature and vitals, including temperature, heart rate and oxygen saturation were monitored throughout the procedure. Prior to incision the scalp was sterilized using betadine and alcohol wipes and a bupivacaine/lidocaine cocktail (1 ml/kg) was administered subcutaneously at the injection site. Bregma-lambda distance was measured and final coordinates were scaled from the atlas distance of 8.7 mm.⁷¹ The coordinates for CA1 were, AP: -3.3/-3.54 mm, ML: 2.2/2.6 mm, DV: 2.35 mm. The final coordinates for CA3b were AP: -3.3/-3.54 mm, ML: 3.0/3.4 mm, DV: 3.45 mm. Virus was loaded into a 10 μ l injection syringe equipped with a 35-gauge beveled NANOFIL needle (World Precision Instruments, Sarasota, FL) and lowered to the target coordinates. Total virus amount was divided and delivered at three depths, DV depth \pm 0.2 mm at a rate of 0.05 μ l/min. All viruses were diluted to $\sim 10^{12}$ vg/ml except for AAV1/hSyn-SIO-stGtACR2-FusionRed which was $\sim 10^{13}$ vg/ml. The following volumes were used for each virus: AAV2/CamKII α -ARCT-GFP (0.5 μ l/site, UNC Vector Core), AAV5/hSyn-oCHIEF-tdTomato (0.3 μ l/site, Duke Viral Vector Core), AAV1/CamKII α -stGtACR2-fusionRed (0.4 μ l/site, Addgene viral prep #105669), AAV1/hSyn-SIO-stGtACR2-FusionRed (0.45 μ l/site, Addgene viral prep #105677). AAV1/CamKII α -stGtACR2 and AAV1/hSyn1-SIO-stGtACR2-FusionRed were gifts from Ofer Yizhar.²⁸ Acute recordings or chronic implantation were performed a minimum of two weeks following virus injection to ensure expression. See [Table S1](#) for a summary of the different experiments.

Anesthetized Recordings

Animals were anesthetized with 1.3 mg/kg urethane (1.3 g diluted into 10 mL saline) plus a supplemental dose of ketamine and xylazine (20 and 2 mg/kg respectively). Additional urethane was administered if signs of inadequate depth of anesthesia persisted, including pedal reflex response. A circular craniotomy was made over dorsal CA1 centered on coordinates, AP: -3.06 mm, ML: 2.0 mm using a 3.7-mm diameter trephine drill bit. For recordings with detached fibers targeting CA3, fibers were attached bilaterally and secured to the skull at coordinates, AP: -4.34 mm, ML: \pm 3.50 mm, DV: 3.45 mm angled $\sim 15^\circ$ anterior to target dorsal CA3b. Electrodes were slowly advanced to the target location (either CA1 or CA3) and allowed 30 minutes to stabilize prior to recording. Recordings typically lasted for ~ 30 min during which light was pulsed at a cycle of either 2-s ON / 8-s OFF, 500-ms ON/ 2-s OFF, or 250-ms ON/ 1-s OFF.

Chronic Recordings

A minimum of two weeks following virus surgery, rats were implanted unilaterally with high-density silicon probes (32 or 64 sites; Buz32 or P-Series; Neuronexus or Cambridge NeuroTech). Probes were attached to a microdrive (modified, see Chung et al.⁷² for basic design) and implanted with a 15° angle along the hippocampal long axis at the following coordinates, AP: -3.06 mm, ML: 2.0 mm. During surgery the tips of the electrodes were lowered to the neocortex at a depth of 1.3 mm. Ground and reference screws were placed in the bone above the cerebellum. Craniotomies were sealed with silicone gel (Dow Corning 3-4680) and wax. To provide physical and electrical shielding, the crown of copper mesh was built around the probe and reinforced with dental acrylic.

Data acquisition

All data, unless otherwise specified, were collected using either Neuralynx Digital Lynx SX data acquisition system with Cheetah software or Intan RHD recording controller with OpenEphys software.⁷³ Analogue neural signals were amplified and recorded at 32 kHz or amplified and digitized on the headstage at 30kHz. Local field potential (LFP) was downsampled to 1250 Hz for additional analysis. For chronic recordings, rat's position was tracked using two LED diodes (red and green), mounted to the headstage and detected by an overhead digital video camera at 30 frames/s. For experiments using detached optic fibers, laser power was measured and set to 10 mW at the end of the cable prior to acquisition. For experiments using either optrodes or μ LEDs, output intensity was set low and gradually increased until changes in cell activity were visually observed. For detached fiber and optrode experiments, light was delivered via a laser (AixiZ; wavelength: 445 nm, oCHIEF/stGtACR2 opsins and 523 nm, ArchT opsin) and output power was controlled using a variable reflective mirror attenuator (NDC-50C-2M, Thorlabs). Integrated μ LED optoelectrodes and the OSC1-LITE μ Driver⁷⁴ used to deliver current to the μ LEDs were furnished by the MINT NeuroNex Technology Hub led by Euisik Yoon, and mounted on 3D printed micro-drives.⁷⁵

Histology

For chronic recordings, a small DC current (2 μ A for 10 sec; A365D, World Precision Instruments) was passed through the deepest electrodes on each shank of the probe prior to sacrificing the animal in order to identify the depth location of a specific recording site. This procedure was not performed for acute recordings since multiple passes were made through both CA1 and CA3 in the same animal. These recordings relied on the depth of electrodes, LFP patterns characteristic to certain layers and responsivity of cells to identify the recording location. The rats were deeply anesthetized using ketamine/xylazine and perfused through the heart first with 0.9% saline solution followed by 4% paraformaldehyde solution. The brains were sectioned by a VT-1000-S Vibratome (Leica,

Germany) at 75 μm in the coronal plane for hippocampus. Sections were mounted on slides, cover-slipped and imaged to verify approximate location of electrodes and virus expression (Figure S1).

Spiking network models

We used spiking network models of conductance-based excitatory and inhibitory neurons described in Sadeh et al.²⁵ to model the CA1 and CA3 regions of the hippocampus using the NEST simulation environment.⁷⁶ Neurons in these networks were modeled using an exponential integrate-and-fire model based on Brette and Gerstner⁷⁷ without the adaptation component. In this model the membrane potential V_m is described by the following first-order differential equation:

$$C \frac{dV_m}{dt} = -g_L(V_m - E_L) + g_L \Delta_T \exp[(V_m - E_T) / \Delta_T] - G_e(t)(V_m - E_e) - G_i(t)(V_m - E_i) \tag{Equation 1}$$

where C is the membrane capacitance, g_L is the leak conductance and E_L is the resting potential. The exponential term reproduces rapid growing of membrane potential during spike generation, where Δ_T is the “slope factor” and E_T is the threshold potential. When the membrane potential V_m reaches E_T , a spike is elicited and the integration of the equation is restarted from a reset value V_r .

The model neurons in these networks are driven via excitatory and inhibitory synaptic inputs represented in the third and fourth terms of Equation 1, respectively. In these terms E_e is the reversal potential of excitatory and E_i is the reversal potential of inhibitory conductances. $G_e(t)$ and $G_i(t)$ are the total excitatory and inhibitory conductances at time t, respectively, defined as:

$$G_e(t) = \sum_j g_e(t - t_j) \tag{Equation 2}$$

$$G_i(t) = \sum_k g_i(t - t_k) \tag{Equation 3}$$

where t_j and t_k are the times when excitatory and inhibitory synaptic events reach a particular post synaptic neuron, respectively. The conductances g_e and g_i map the timing of synaptic events onto changes in the membrane conductance based on the following equations:

$$g_e(t) = H(t)J_e \exp(1 - t / \tau_e)t / \tau_e \tag{Equation 4}$$

$$g_i(t) = H(t)J_i \exp(1 - t / \tau_i)t / \tau_i \tag{Equation 5}$$

Neural dynamics parameters used in neural network simulations of CA1 and CA3

Parameter	Symbol	Value
Membrane capacitance	C	120 pF
Reversal potential of excitatory conductances	E_e	0 mV
Reversal potential of inhibitory conductances	E_i	-75 mV
Resting potential	E_L	-70 mV
Spiking threshold voltage	E_T	-50 mV
Slope factor	Δ_T	2 ms
Leak conductance	g_L	7.14 nS
Refractory period	t_{ref}	2 ms
Rise time of excitatory conductances	τ_e	1 ms
Rise time of inhibitory conductances	τ_i	1 ms
Reset voltage	V_r	-60 mV

Network parameters used in neural network simulations of CA1 and CA3, except where specified otherwise.

Parameter	Symbol	Value	
		CA1	CA3
Connection probability from CA3 exc. to CA1 exc.	$CP_{CA3e-CA1e}$	0.05	0.05
Connection probability from CA3 exc. to CA1 inh.	$CP_{CA3e-CA1i}$	0.05	0.05
Connection probability from exc. to exc.	CP_{e-e}	0.14	0.4
Connection probability from exc. to inh.	CP_{e-i}	0.45	0.15
Connection probability from inh. to exc.	CP_{i-e}	1	1

(Continued on next page)

Continued

Parameter	Symbol	Value	
		CA1	CA3
Connection probability from inh. to inh.	CP_{i-i}	1	1
Peak conductance of background input	J_{bkg}	0.1 nS	0.1 nS
Mean peak conductance from CA3 exc. to CA1 exc.	$J_{CA3e-CA1e}$	0.02 nS	0.02 nS
Mean peak conductance from CA3 exc. to CA1 inh.	$J_{CA3e-CA1i}$	0.1 nS	0.1 nS
Mean peak excitatory conductance	$J_{e-\gamma}$	0.22 nS	0.03 nS
Mean peak inhibitory conductance	$J_{i-\gamma}$	-0.3 nS	-0.3 nS
Firing rate of background input to excitatory cells	ν_{bkg_e}	9500 Hz	9600 Hz
Firing rate of background input to inhibitory cells	ν_{bkg_i}	7000 Hz	9600 Hz
Reduction of background input firing rate mimicking photoinhibition	ν_{pert}	-400 Hz	-400 Hz

where $H(t)$ is the Heaviside step function, J_e denotes the peak excitatory conductance and J_i denotes the peak inhibitory conductance. τ_e and τ_i are the rise times of excitatory and inhibitory postsynaptic conductances, respectively.

We modeled two neuron populations representing CA1 and CA3. Each population consists of excitatory (e) and inhibitory (i) subpopulations of size N_e and N_i , respectively, that are randomly connected using a binomial distribution with a mean connection probability of $CP_{X-\gamma}$ from subpopulation X to subpopulation Y. The peak conductance of each connection is random and drawn from a Gaussian distribution with the mean $J_{X-\gamma}$ and the standard deviation $J_{X-\gamma}/5$. To be consistent with Dale's law, we set any negative weights for excitatory connections and positive weights for inhibitory connections to zero.

CA1 and CA3 each consists of $N_e = 1600$ excitatory and $N_i = 400$ inhibitory neurons. In our model, CA3 featured a higher excitatory-to-excitatory connection probability compared to CA1. To ensure an overall balance of excitatory and inhibitory activity in this network, so that inhibitory stabilization did not shut down all excitatory activity, we also heuristically reduced the excitatory-to-inhibitory connectivity (CP_{e-i}) and the peak conductance of excitatory inputs ($J_{e-\gamma}$) in CA3, as compared to CA1.

Between the two populations, CA3 excitatory neurons project to CA1, forming a feed-forward network. The connections of these feed-forward projections were also drawn from a binomial distribution with mean connection probability $CP_{CA3e-CA1,Y}$. The corresponding peak conductances were drawn from a Gaussian distribution with mean $J_{CA3e-CA1,Y}$ and standard deviation $J_{CA3e-CA1,Y}/5$, where negative weights were set to zero.

Neurons in the model also received excitatory input from independent homogeneous Poisson spike trains firing at rate ν_{bkg_e} and ν_{bkg_i} to the e and i population, respectively, with a peak conductance of J_{bkg} , included in the sum in equation 2, to model background inputs from other brain areas such as the entorhinal cortex. The effect of photoinhibition was modelled by reducing the background input rate to both subpopulations in CA3 or CA1 by ν_{pert} . Modeling results were obtained by simulating 10 different instances of the model (different initializations of the connectivity matrix) and each model 10 times with different realizations of the inputs. The outcomes were then averaged across the 100 simulations.

A signature of an inhibition-stabilized network (ISN) is that it becomes unstable in the absence of inhibition.^{12,25} To confirm that our networks models operate in an ISN regime, we performed additional simulations where we clamped the peak inhibitory conductance $J_{i-\gamma}$ to 0 in CA1 and CA3 separately (Figure S7). We computed the average firing rate of the network as a function of the peak excitatory conductance and checked whether the firing rate explodes in the absence of inhibition. To determine how high a firing rate corresponds to unstable activity, we looked at the changes of firing rate and identified the peak excitatory conductance above which the firing rate increased abruptly. If the peak excitatory conductance of the model was above this threshold, we classified the network as an ISN.

QUANTIFICATION AND STATISTICAL ANALYSIS

Data processing and cell classification

Raw signal was high-pass filtered and waveform extraction and initial clustering was conducted using SpikeDetekt and KlustaKwik.⁷⁸ Further manual adjustment of the clusters was then performed using Klusters.⁷⁹ Only well isolated units, defined by clear refractory periods and well-defined cluster boundaries were included in analysis. A subset (~15 %, 478/3481 recorded cells) of putative pyramidal and putative interneuron cell types were initially categorized visually using firing rate and features of the autocorrelograms (Figure S2). Quadratic discriminant analysis (R software) was then used to classify the remaining cells as either putative pyramidal or putative interneurons. Four variables were used for classification: waveform asymmetry, waveform trough to peak, cell burstiness and firing rate.^{80,81} The discriminant analysis perfectly separated the training group. 37 cells did not meet our criterion of having a posterior probability between 0.1 and 0.9 and were excluded from further analysis.

Cell response statistics

All analyses were performed using custom MATLAB (Mathworks, Natick, MA) code. Laser pulse epochs either following behavior or during the anesthetized recording were used for cell response evaluation. For each cell, spiking activity was aligned to the onset of the laser. A 20-ms window centered on the stimulation onset was excluded from analysis to avoid possible inflation of firing rates resulting from light artifacts. In order to account for neuron instability, especially during anesthetized recordings, analysis was restricted to trials with firing rate > 0 . Baseline (OFF) was considered to be the time window immediately prior to illumination with a duration equal to the duration of illumination. Firing rates were calculated as the total number of spikes in the baseline and stimulation windows divided by the duration of the corresponding window. A binomial test on total spike count was used to determine whether individual cells responded significantly to optogenetic perturbation. Cells with $p < 0.01$ were considered responsive. Mean ΔFR was used to determine the direction and degree of responsiveness.

To compare these results with a null distribution, we performed a parallel set of analyses where we compared the baseline (OFF) period with the equivalent duration OFF window immediately preceding it. We performed the same tests as for the data on these two OFF windows, therefore obtaining a null distribution of the cell responses that can potentially produce false positives due to chance, instabilities, and drift in the data. Results from these analyses are provided in [Figures S3](#) and [S4](#). To test whether the proportions of cells that showed paradoxical responses (i.e. increased firing except for [Figure 4](#), where decreased firing was paradoxical) were significantly higher than chance, we compared the proportions extracted from our data with the proportions observed in the surrogate “baseline null” dataset using Fisher’s exact tests. Note that because this is a permutation test, we do not report an associated test statistic—only the p-value. Results of all comparisons between experimental and baseline nulls are reported in [Table S2](#) (See also [Table S3](#)).